

INFRASONIC IMPEDANCE MEASUREMENTS OF BUILDINGS
FOR AIR LEAKAGE DETERMINATION

by

Richard W. Graham

B.Sc. (E.E.) Syracuse University, 1975

Technical Report TR-77-15

NSF Grant ENG-75-23416

THESIS

Submitted in partial fulfillment of the requirements for the degree
of Master of Science in Computer Engineering in the Graduate School
of Syracuse University, May 1977.

Department of Electrical and Computer Engineering
Syracuse University
Syracuse, NY 13210

June 1977

ABSTRACT

Air leakage (infiltration) accounts for 30% or more of the heating loads in some residential housing units. Available air leakage testing procedures using tracer gas techniques, or pressure drop versus flow caused by a blower, are costly, time-consuming and require the use of bulky apparatus. Moreover, the results may depend on weather conditions.

This thesis reports on preliminary research directed towards developing a new method for measuring the air leakage property of an enclosure such as a building. By the new infrasonic method, the low-frequency (0.1 to 10 Hz) acoustic impedance of the enclosure is measured. Under typical conditions the real part of the acoustic admittance (reciprocal of impedance) provides the flow-versus-pressure property of the enclosure. The thesis describes and analyses a diaphragm-type motor-driven source and a pressure sensor with electronic filters used to measure infrasonic impedance.

The infrasonic impedance results were compared to blower measurements for the same enclosures. For enclosures of volume less than 57m^3 (2000ft.^3), the disagreement between the two methods was less than 10%. On larger enclosures, data from both testing methods were more scattered and some results differed by more than a factor of three. However, we have demonstrated that the infrasonic impedance of a building can be measured and used to determine the building's air leakage properties. It is hoped that refinements in our present equipment, in progress now, will improve the data for the larger enclosures.

PREFACE

The work contained in this thesis is part of a broader program of energy concern at Syracuse University. Under the direction of W. Howard Card, I have had the opportunity to study many facets of energy use, and the alternate forms that are now starting to be taken seriously. It is hoped that we may have laid the groundwork for a testing procedure for air infiltration in buildings that will soon be helpful in the conservation efforts of the U.S.

The research for this thesis was supported by the Syracuse University Senate Research Committee (1975-76) and the National Science Foundation (1976-77)* with W. Howard Card as principal investigator.

I would like to thank Dr. Card for his help and point out that most of the preliminary work and theory should be credited to him. A grateful thanks to Steve Franz, Bill Thompson and T. R. Nash for their help and encouragement. Lastly, a special thanks to Karen Raab for her time and patience in typing the thesis.

* National Science Foundation Grant number ENG75-23416.

TABLE OF CONTENTS

	Page
PREFACE	ii
TABLE OF CONTENTS	iii
CHAPTER I	
INTRODUCTION	1
CHAPTER II	
THEORY OF THE INFRASONIC IMPEDANCE METHOD	4
2-1 Dynamic Pressure-Flow Relationships	4
2-2 Frequency Response-Linear Analysis	14
2-3 Frequency Response-Nonlinear Analysis	17
CHAPTER III	
EQUIPMENT	21
3-1 Source Equipment	21
3-2 Pressure Sensor Equipment	22
3-3 Pressure Sensor Electronics	25
CHAPTER IV	
TEST RESULTS	27
4-1 Test Locations	27
4-2 Infrasonic Impedance Tests	27
4-3 Blower Test Results	36
4-4 Discussion of Results	36
CHAPTER V	
PRESENT WORK AND RECOMMENDATIONS	40
5-1 Experimental Work and Recommendations	40
5-2 Theoretical Work and Recommendations	40

CHAPTER VI	
CONCLUSION	41
APPENDIX A	
SOLUTION OF EQ. (2-13)	42
APPENDIX B	
VOLUMETRIC FLOW SOURCE AND EQUIPMENT	44
APPENDIX C	
SIGNAL PROCESSING CIRCUIT	48
REFERENCES	53

I. INTRODUCTION

The recent rise in the cost of energy and the severe shortage of natural gas along with our growing dependence on foreign countries for oil make it imperative that we find ways of conserving and wisely using our dwindling energy supplies. In 1974 nearly 11% of our total energy use was for residential space heating [Ref. 1]*. Studies have shown that residential energy use will continue to rise despite efforts to turn the trend downward. Although most of the residential heating load is due to conductive losses, 30% or more of the total load can be accounted for by direct exchange of warm inside air for cold outside air. This process is commonly known as "air infiltration" [Ref. 2,3,4]. As the insulation quality of a building increases so does the proportion of the heating and cooling load associated with air infiltration, even though the total heating and cooling load will decrease.

There is a need for fresh air in almost all buildings; however the supply of fresh air for a building is seldom controlled directly, but instead depends largely on the surrounding environment. Indoor-outdoor temperature differences, wind speed and wind direction combined with poor quality workmanship in construction account for the major causes of residential air infiltration. While good insulation practices and detailed plan specifications can do an excellent job of cutting conductive loss, quality of workmanship remains the dominant factor determining the amount of air leakage even in well-designed buildings. As a consequence of these factors, the air infiltration level is often 2 or 3 times the amount of fresh air actually needed.

There is a great need for a good method of obtaining flow versus pressure characteristics of buildings. At this time, no simple pro-

* References on pages 53-54.

cedure exists for a designer or builder to check the quality of the workmanship of a new building for the amount of air infiltration. In addition, better estimates of thermal performance improvement could be obtained with a cheap, fast method of determining the amount of air infiltration in older buildings.

The presently available methods for air leakage measurements are not highly developed. Infiltration meters using tracer gas methods are in developmental stages, but measurement results depend somewhat on weather conditions. Accurate results can be obtained by the blower method, although the test equipment is awkward to use and the testing is very time consuming. This method typically requires the mounting of a blower connected to the building exterior and the measurement of air flow (for example by an orifice plate or nozzle) for various building static pressures. Results can vary depending on operator skill and care in making delicate pressure measurements.

The infrasonic impedance method of testing, under study here, measures the low-frequency acoustic impedance of an enclosure such as a house. Basically, by applying slowly changing pressure differences (typically in the frequency range of 0.1 to 10 Hz), we can obtain a dynamic measurement of the building acoustic impedance. The real part of the admittance (reciprocal of impedance) is the important parameter to determine the amount of air infiltration. To date, we know of no other work that has been done with low-frequency acoustic building impedance for the determination of air leakage, or for any other purpose. Several curious effects have surfaced in our testing. Future study may well provide interesting results of building properties, as well as a useful method to determine the amount of air infiltration.

The purpose of our work, then, was to design, build, and evaluate an instrumentation system to determine building impedance in order to find building air leakage properties.

II. THEORY OF THE INFRASONIC IMPEDANCE METHOD

2-1 Dynamic Pressure - Flow Relationships

We can gain a basic understanding of the mechanical aspects of the infrasonic impedance measuring system from a simple description. An electrical analogy can then be drawn and a system model developed. For an enclosure such as a room, air alternately pumped in and pulled out in a very low-frequency sinusoidal fashion could act as our excitation. (We would call such a pump a vented pump because it obtains air from and discharges air to the atmosphere). If there are no leaks in the enclosure the response to the excitation would be a sinusoidal pressure change within the whole enclosure proportional to the amplitude of the excitation and inversely proportional to the volume of the enclosure. If we then considered laminar flow leaks in the enclosure, we would see that the response decreased proportionally to the leak size. The response for turbulent flow leaks would not be exactly proportional to the pressure differential, but analysis of turbulent flow leaks will be shown to be a variation of the laminar flow case.

Figure 1 shows a schematic representation of the dynamic air leakage test equipment. Photographs of the actual equipment are shown in Fig. 2 and Fig. 3. Our pump, while providing the same effect as a vented pump, was not vented externally but merely compressed and rarified the air in the container inside the enclosure and thus respectively rarified and compressed the air of the remainder of the enclosure. The elimination of external venting reduces the complexity of equipment set up, which is a major drawback of the blower method of testing.

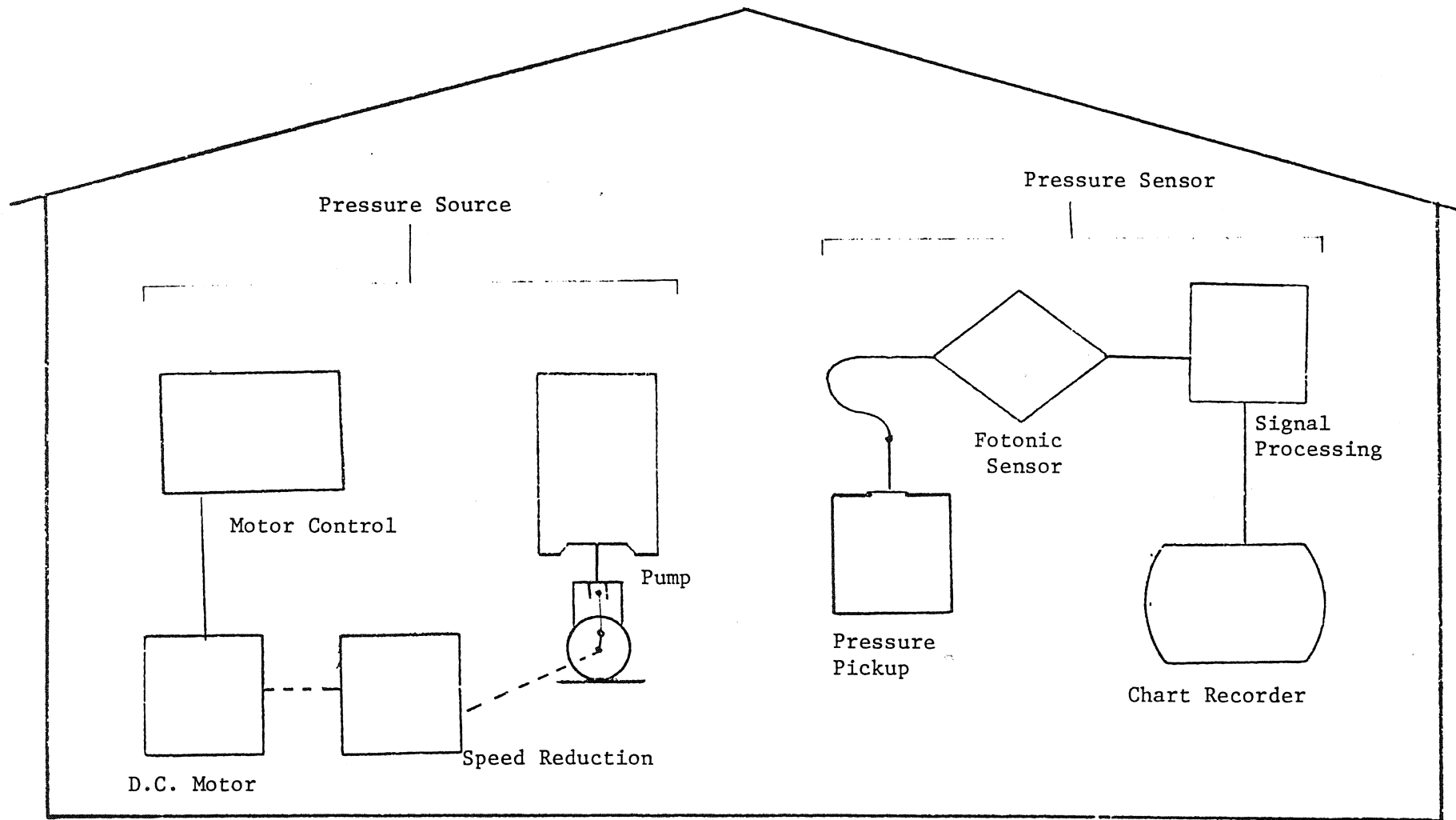


Fig. 1 Schematic diagram of infrasonic impedance measuring equipment.

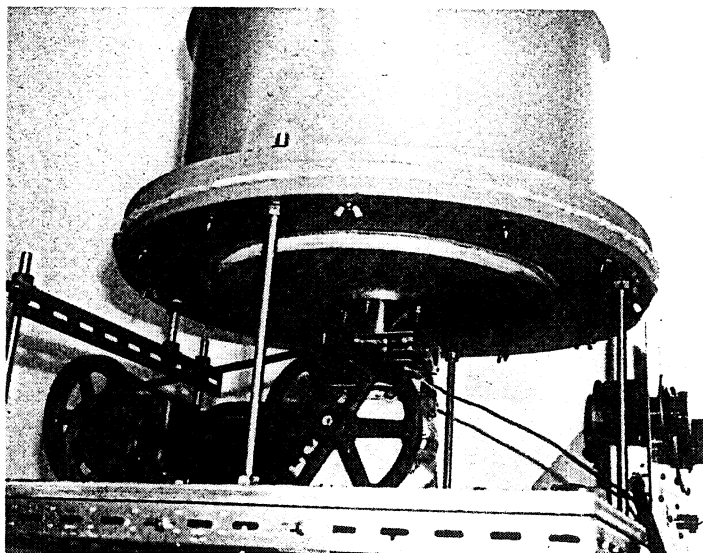
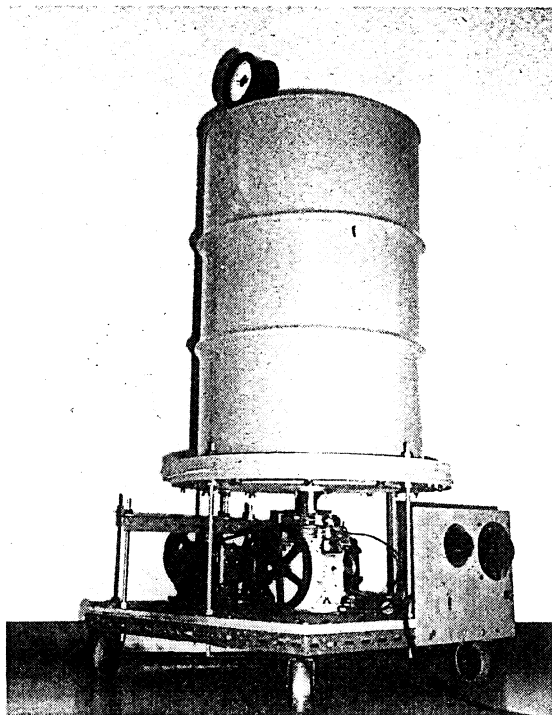


Fig. 2. Photographs of pressure source equipment.

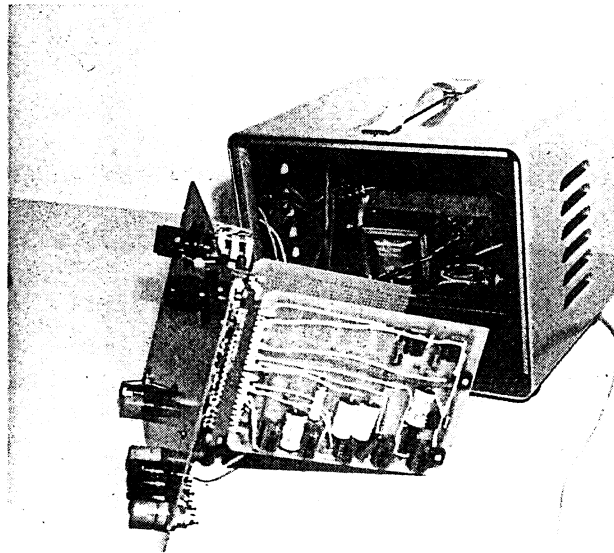
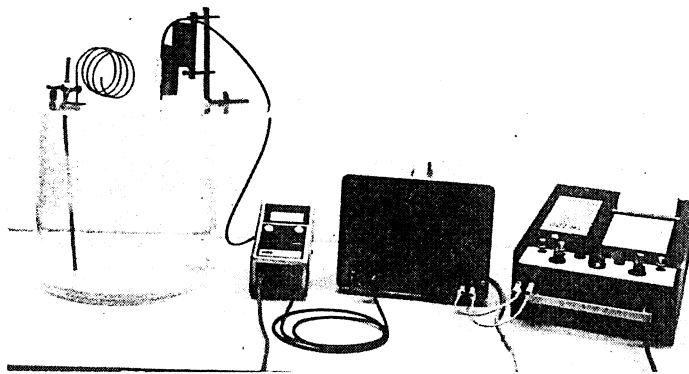


Fig. 3. Photographs of pressure pickup equipment and electronics.

The variable-speed-drive reciprocating piston (Fig. 1) gives a nearly sinusoidal excitation of the form*

$$v_s(t) = V_s \sin \omega t \quad (2-1)$$

where V_s represents one-half the pump displacement and ω is the angular speed of the pump. Differentiating Eq. (2-1) provides the volume flow rate of the source

$$q_s(t) = \frac{dv_s}{dt} = V_s \omega \cos \omega t \quad (2-2)$$

Thus the amplitude of the volumetric flow source is

$$Q_s = V_s \omega \quad (2-3)$$

Some idea of the concept of capacitance as it relates to the volume of an enclosure such as a building can be obtained if one thinks of the "springy" effect of air. As air is pumped into an enclosure the pressure increases just as a spring decreases in length when compressed. Both enclosure and spring can be modelled by an electrical capacitance [Ref. 5]. As long as the linear dimensions of an enclosure are small compared to the wavelength of the infrasonic excitation, a lumped parameter approach is valid. Enclosure capacitance can then be defined as

$$C = \frac{\Delta V}{\Delta P} \quad (2-4)$$

where a decrease in volume, ΔV , causes an increase in pressure, ΔP . Provided we have a reversible adiabatic condition (a good approximation),

* (Note: All symbols, units and definitions used in the text are provided in Table I, page 9).

TABLE I
SYMBOLS AND UNITS

	<u>Description</u>	<u>SI Units</u>	<u>Common Units</u>
A_d	Pickup diaphragm area	m^2	ft^2
C	Acoustic capacitance	m^5/N	ft^5/lb
G	Electrical conductance	mho	mho
K	Air leakage parameter		
K_1	Air leakage parameter	$m^5/N\text{-sec}$	$ft^5/lb\text{-min}$
P	Atmospheric pressure	N/m^2	lbs/ft^2
Q	Volumetric flow rate	m^3/sec	ft^3/min
Q_s	Volumetric source amplitude	m^3/sec	ft^3/min
S_b	Back side Fotonic sensor sensitivity	m/V	$\mu in/mV$
S_f	Frontside Fotonic sensor sensitivity	m/V	$\mu in/mV$
V	Enclosure or building volume	m^3	ft^3
V_P	Volume of pickup chamber	m^3	ft^3
V_s	Half of source displacement	m^3	ft^3
$e(t)$	Voltage	volts	
$i_c(t)$	Capacitance current	amperes	
$i_g(t)$	Conductance current	amperes	
$i_s(t)$	Source current	amperes	
n	Air leakage exponent		
$q_c(t)$	Volumetric capacitance flow	m^3/sec	ft^3/min
$q_g(t)$	Volumetric leakage flow	m^3/sec	ft^3/min

TABLE I (Cont'd)

$q_s(t)$	Volumetric source flow	m^3/sec	ft^3/min
v_f	Fotonic sensor voltage	volts	
$v_s(t)$	Source volume function	m^3	ft^3
γ	Adiabatic exponent		
ΔP	Incremental change of pressure	N/m^2	lb/ft^2
ΔV	Incremental change of volume	m^3	ft^3
$\Delta p(t)$	Time varying pressure difference	N/m^2	lb/ft^2
Δp_m	Sinusoidal pressure difference amplitude	N/m^2	lb/ft^2
ϕ	Angle that pressure lags flow	radians	
ω	Source shaft speed	rad/sec	
ω_1	Break-point frequency (linear)	rad/sec	
ω_2	Break-point frequency (general)	rad/sec	

$$PV^\gamma = \text{Constant} \quad (2-5)$$

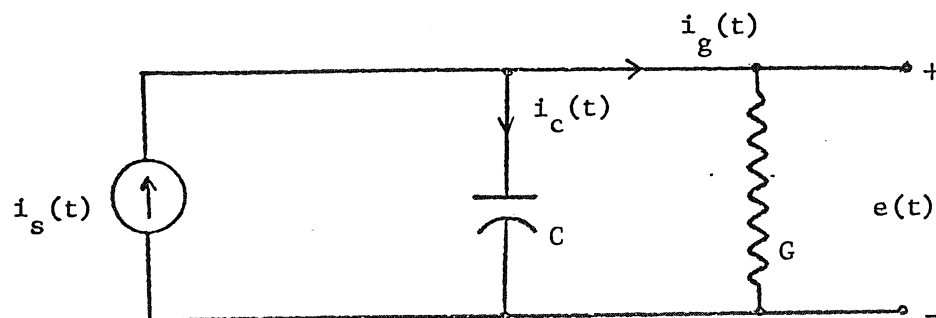
where P is the pressure, V is the volume and γ is 1.401 (the ratio of specific heats for air). It can then be shown from Eqs. (2-4) and (2-5) that

$$C = \frac{V}{\gamma P} \quad (2-6)$$

For the very small pressure changes we are dealing with, P remains essentially constant at atmospheric pressure and, as expected, the capacitance is proportional to the volume.

In much the same way that volumes of air can be modelled as electrical capacitors, leaks in enclosures can be modelled as electrical resistors. The model becomes somewhat more complicated here as the resistance to flow is usually nonlinear and depends on the dimensions of the openings. In addition, associated with the mass of air moving through an opening, there is an inductive effect which is also dependent on the dimensions of the openings. Our lumped parameter approach makes an exact theoretical formulation of resistance and inductance impossible, but the concepts allow useful analyses to be applied to our model for predicting behavior and interpreting results. Formulations for certain geometries of leaks and conditions have been developed for resistances and inductances [Ref. 6]. In general, our basic circuit model of an enclosure such as a building will be as shown in Fig. 4. This will be modified to show new parameters as they become important or to explain certain experimentally observed results.

If we now look at the response of an enclosure to a sinusoidal volume flow input time-varying pressure $\Delta p(t)$, using Eq. (2-4) we obtain



Analogous Quantities

Electrical	Mechanical
$i_s(t)$	$q_s(t)$
$i_c(t)$	$q_c(t)$
$i_g(t)$	$q_g(t)$
C	C
G	K or K_1
$e(t)$	$\Delta p(t)$

Fig. 4. Electric circuit model of building parameters.

$$\Delta p(t) = \frac{1}{C} v_s(t) \quad (2-7)$$

Differentiating Eq. (2-7) and substituting in Eq. (2-2) yields

$$\frac{d}{dt} \Delta p(t) = \frac{1}{C} \frac{d}{dt} v_s(t) = \frac{1}{C} q_s(t) \quad (2-8)$$

If we assume the enclosure to be tightly sealed, then all the air flow is into the enclosure (no leakage) and $q_s(t)$ becomes $q_c(t)$ so that

Eq. (2-8) now becomes

$$q_c(t) = C \frac{d}{dt} \Delta p(t) \quad (2-9)$$

which is the relationship of flow and pressure for an acoustic capacitance. Equation (2-9) is analogous to the current-voltage relationship for electrical capacitors where $q_c(t)$ is analogous to current, and $\Delta p(t)$ is analogous to voltage.

Previously it was indicated that the individual leaks in a building would be difficult to model theoretically and, in fact, actual experimental results differ from predicted results [Ref. 7]. An equation of the general form

$$Q = K (\Delta p)^n \quad (2-10)$$

has been shown to provide a close approximation of the flow (Q) for real buildings [Ref. 8]. In Eq. (2-10) Q and Δp are steady state volume flow rate and pressure difference, respectively. Usually n is in the range of 1/2 to 1, and K is an experimental constant. Fully developed laminar flow yields $n = 1$. When applying sinusoidal time-varying excitations Eq. (2-10) becomes

$$q_g(t) = K \frac{\Delta p(t)}{|\Delta p(t)|} |\Delta p(t)|^n \quad (2-11)$$

where $q_g(t)$ is the time-varying leakage flow rate for an enclosure having negligible volume. Provision is made not to take the root of a negative number in Eq. (2-11) by utilizing the magnitude of the differential pressure and obtaining flow direction by the factor $\Delta p(t)/|\Delta p(t)|$.

By combining Eqs. (2-9) and (2-11) we find the effect on an enclosure with both volume and leakage. Then

$$q_c(t) + q_g(t) = q_s(t) \quad (2-12)$$

and by substitution

$$C \frac{d}{dt} \Delta p(t) + K \frac{\Delta p(t)}{|\Delta p(t)|} |\Delta p(t)|^n = q_s(t) \quad (2-13)$$

which is, in general, a nonlinear differential equation. A closed form solution is not easily obtainable for this equation. However, by examining the limiting cases and by approximation we will gain some insight into the expected results.

2-2 Frequency Response - Linear Analysis

If we first consider Eq. (2-13) when $n = 1$ (laminar flow), and for this special case designate $K = K_1$, then

$$C \frac{d}{dt} \Delta p(t) + K_1 \Delta p(t) = q_s(t) \quad (2-14)$$

Substituting Eq. (2-2) into Eq. (2-14) yields

$$C \frac{d}{dt} \Delta p(t) + K_1 \Delta p(t) = V_s \omega \cos \omega t \quad (2-15)$$

This is a linear first-order differential equation.

Analysis of Eq. (2-15) yields a steady-state solution of the form

$$\Delta p(t) = \Delta p_m \cos(\omega t - \phi) \quad (2-16)$$

where Δp_m is half the peak-to-peak variation in $\Delta p(t)$ and is given by

$$\Delta p_m = \frac{V_s \omega}{[K_1^2 + (\omega C)^2]^{1/2}} \quad (2-17)$$

and

$$\phi = \tan^{-1} \frac{\omega C}{K_1} \quad (2-18)$$

Equation (2-16) provides our expected sinusoidal waveform for $\Delta p(t)$. K_1 (the real part of the acoustic admittance) is the parameter containing the air leakage information.

A convenient form in electrical engineering for this type of response is a Bode plot, which is a plot of the logarithm of amplitude versus the logarithm of frequency. Figure 5 shows a normalized Bode plot for $n = 1$ and gives the expected frequency response of buildings having laminar flow leakage. At high frequencies the capacitance dominates so that Eq. (2-17) simplifies to

$$\Delta p_m = \frac{V_s}{C} \quad (2-19)$$

This is understood by realizing that at high frequencies of excitation, the air is alternately compressed and rarified and has very little time to leak in and out. At very low frequencies, however, the leakage becomes dominant and very little capacitive effect is noted and so Eq.(2-17) simplifies to a straight line on the Bode plot

$$\Delta p_m = \frac{V_s}{K_1} \omega \quad (2-20)$$

It is this portion of the curve, the low frequency asymptote, where our air leakage data lies since it contains the factor K_1 while the high frequency asymptote, Eq. (2-19), depends only on the capacitance for

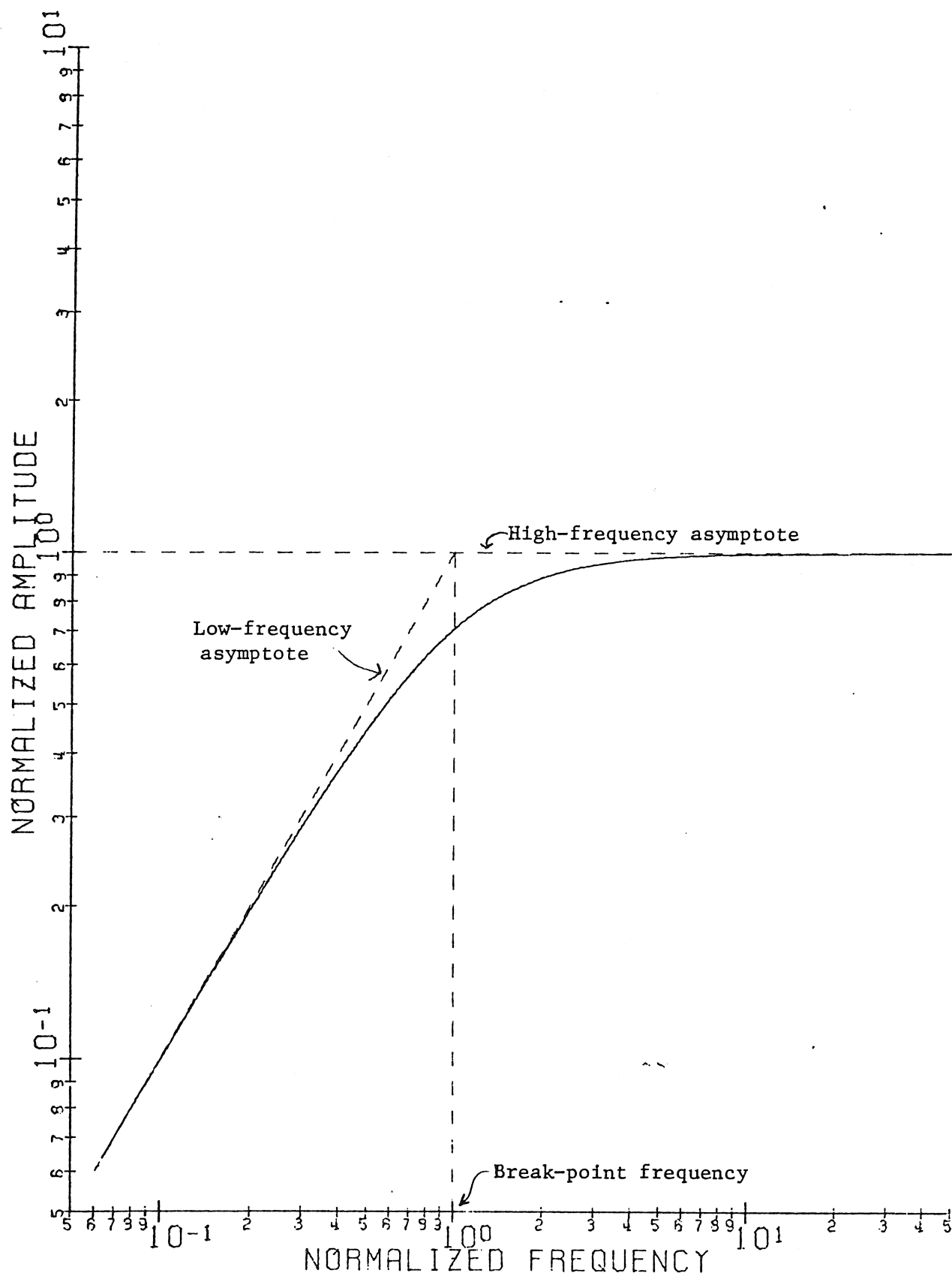


Fig. 5. Theoretical normalized linear response.

a given excitation. Moreover, this result shows that under the assumed conditions, air leakage measurements must be made at relatively low frequencies, typically less than one Hertz.

The break frequency (ω_2) we define as the frequency of the intersection of the low frequency asymptote Eq. (2-20) with the high frequency asymptote, Eq. (2-19). The break frequency is shown on our normalized graph, Fig. 5.

2-3 Frequency Response - Nonlinear Analysis

Following the same approach as in the linear case ($n = 1$), we shall approximate a solution for the nonlinear equation, ($n \neq 1$), of Eq. (2-13). In the high-frequency situation, the capacitive term will again dominate and so we obtain the same asymptote as for the linear case. At low frequencies, the capacitive effect can be neglected and we are left with

$$K \frac{\Delta p(t)}{|\Delta p(t)|} |\Delta p(t)|^n = V_s \omega \cos \omega t \quad (2-21)$$

Realizing that the positive and negative extremes have the same magnitude, we will look only at the positive extreme of $\Delta p(t)$ so that

$$K |\Delta p(t)|_{\max}^n = V_s \omega \quad (2-22)$$

then

$$|\Delta p(t)|_{\max} = \left[\frac{V_s \omega}{K} \right]^{\frac{1}{n}} \quad (2-23)$$

Taking the logarithm of both sides of Eq. (2-23) yields

$$\ln |\Delta p(t)|_{\max} = \ln \left[\frac{V_s}{K} \right]^{\frac{1}{n}} + \frac{1}{n} \ln \omega \quad (2-24)$$

Plotted on log-log paper then we expect a straight line with a slope of $1/n$. The value of n obtained from a Bode plot of experimental results gives us some indication of the type of flow (laminar or turbulent) which we could expect to find in the openings in the enclosure. However, our main objective is to establish a good method of finding K , our air leakage parameter. Our Bode plots take on the shape of an ideal single-pole high-pass filter in the laminar flow (linear) case. The break frequency in the linear case occurs when

$$\omega_1 = \frac{K_1}{C} \quad (2-25)$$

and in the nonlinear case when

$$\omega_2 = \frac{K}{C^n V_s^{1-n}} \quad (2-26)$$

We see that the nonlinear case reduces to the linear case when $n = 1$ as expected.

The details of the numerical solution of Eq. (2-13) can be found in appendix A. Figure 6 shows plots of our approximate solution to Eq. (2-13) for different values of n .

The application of Eq. (2-26) allows us to determine our value of K and thus the air leakage from a given enclosure. The basic procedure is as follows:

1. Measure the enclosure dimensions for determination of volume.
2. Determine volume of excitation signal V_s (standard volume source remains the same for all tests).
3. Run a frequency response of the enclosure.
4. Plot output (Bode plot).
5. Determine break frequency (ω) and n .

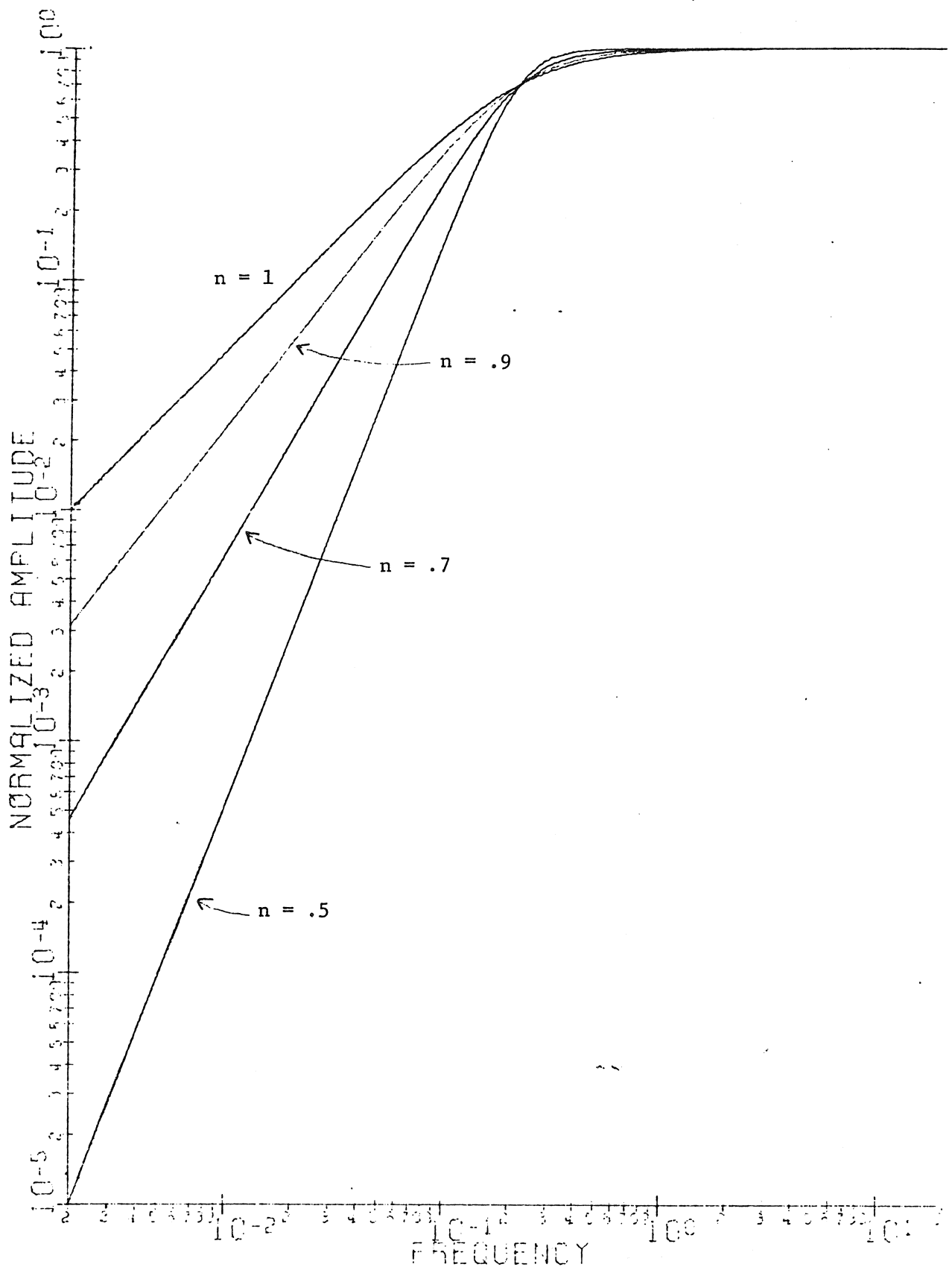


Fig. 6. Change in slope of low frequency asymptote as n decreases, approximate solution.

6. Calculate leakage parameter from formula, Eq. (2-26).

In general step 2 need only be done once and step 1 can be eliminated altogether if the frequency response is run high enough to get onto the "flat" portion of the Bode plot. Usually, however, a volume estimate is made as a system check.

III. EQUIPMENT DEVELOPMENT

Work in the area of low-frequency atmospheric pressure changes has been very limited, consequently we know of no suitable equipment on the market which fills our needs. Calculations showed that the equipment needs to operate over a range of about 0.1 to 10 Hertz with a source displacement (V_s) of at least 0.003 M^3 (.1 cubic feet). More displacement might be needed for larger structures and in areas of high interference from noise. A pressure sensor sensitive enough to detect changes of 0.12 N/M^2 (5×10^{-4} inches of water) or less was needed in leaky buildings for low frequencies and small pump displacement. This is more than 250 times the sensitivity of a typical barometer. These specifications are not rigid, but serve mainly as a guide in our equipment development. Trade-offs, such as a decrease in pickup sensitivity being offset by a larger source volume, could be made where needed. In principle, the use of a more sensitive pickup permits the use of a smaller source displacement.

3-1 Source Equipment

The volumetric flow excitation signal was provided by a d-c motor driven diaphragm pump shown schematically in Fig. 1. A scale drawing, equipment specifications and the motor control circuit diagram are provided in Appendix B. Flexibility in pulley ratios and voltage control of the d-c motor allowed a frequency range of 0.1 to 10 Hertz. The crank mechanism (from a 3 H.P. lawnmower engine) provided a nearly sinusoidal diaphragm motion. Our source displacement was determined by multiplying the diaphragm area by one-half the stroke of the crank mechanism. Because of the construction the source displacement is not adjustable. A diaphragm, as opposed to a piston type pump, was used to

prevent leakage of air between the inside of our rigid container (55 gallon drum) and the outside when the air inside was compressed or rarified.

3-2 Pressure Sensing Equipment

Microbarographs have been developed using chambers on both sides of a thin diaphragm with capillary tubes connecting both chambers to the atmosphere [Ref. 9]. The chambers act as acoustic capacitances and the capillary tubes as the resistances. Together they provide mechanical filtering of the atmospheric pressure changes applied to the diaphragm. By correct adjustment of the capillary tubes, any frequency range of interest may be observed. Utilizing this concept our pressure sensor contains a single chamber and one slow leak to provide a single-pole, high-pass filter characteristic. This high-pass characteristic helps block slow changes in barometric pressure and noise at frequencies below 0.05 Hertz which might otherwise obscure the excitation signal. Ideally we would like a much sharper high-pass characteristic (more poles) than is provided by the mechanical filter but this is not easily achieved mechanically.

Diaphragm displacement can be sensed several ways. Capacitive coupling (electrical) and optical sensing are the two methods that are easiest to use and are the most accurate. We chose the optical sensing method for the simplicity and flexibility it provided in the choice of pickup diaphragm material. A depth-sensing light probe called a Fotonic sensor (See equipment section Appendix B) allowed diaphragm displacements as small as one microinch to be measured. The pressure sensor was designed to allow the chamber volume behind the diaphragm to be varied, thus keeping diaphragm displacement in the linear range of the optical sensor.

This allows adjustment to be made for buildings of different volumes.

The Fotonic sensor has a characteristic curve shown in Fig. 7. The back side (negative sloping) portion of the curve has a nearly constant slope between 30 and 55 mils (distance between light probe and diaphragm). This region of constant slope is referred to as the back side linear range of the Fotonic sensor. The sensitivity (S_b) in this region is 116.0 microinches per millivolt. The front side (positive sloped portion) of the curve has a linear region of greater sensitivity ($S_f = 5.8$ microinches per millivolt) but this was used in only a few tests. The pickup diaphragm displacement was so large in most cases, the diaphragm moved out of the linear range of the front side causing nonlinear signals. Care was taken on back side measurements to keep the pressure sensor chamber volume small enough to remain in the linear region and large enough for a reliable signal.

For our smaller volume enclosures (less than 50 m^3), we used a pickup volume of $.0062 \text{ m}^3$ and for the larger enclosures (greater than 50 m^3), a pickup chamber volume of $.018 \text{ m}^3$ gave us a small enough reliable signal. We found that operating over less than half the linear range assured us that no noise signal superimposed on the source signal would drive the Fotonic sensor into the nonlinear regions.

The diaphragm used in the pressure pickup was mounted over a 4 inch diameter hole using a thin grease film. Since our pickup displacement is caused by the compressibility of the chamber air, it was necessary that the diaphragm be ideally massless and have zero elasticity. The use of the grease film to hold a very thin ($1 \times 10^{-5} \text{ m}$) plastic diaphragm material allowed the diaphragm tension to be held at a minimum and the mass to be negligible. We shall call this type of setup a

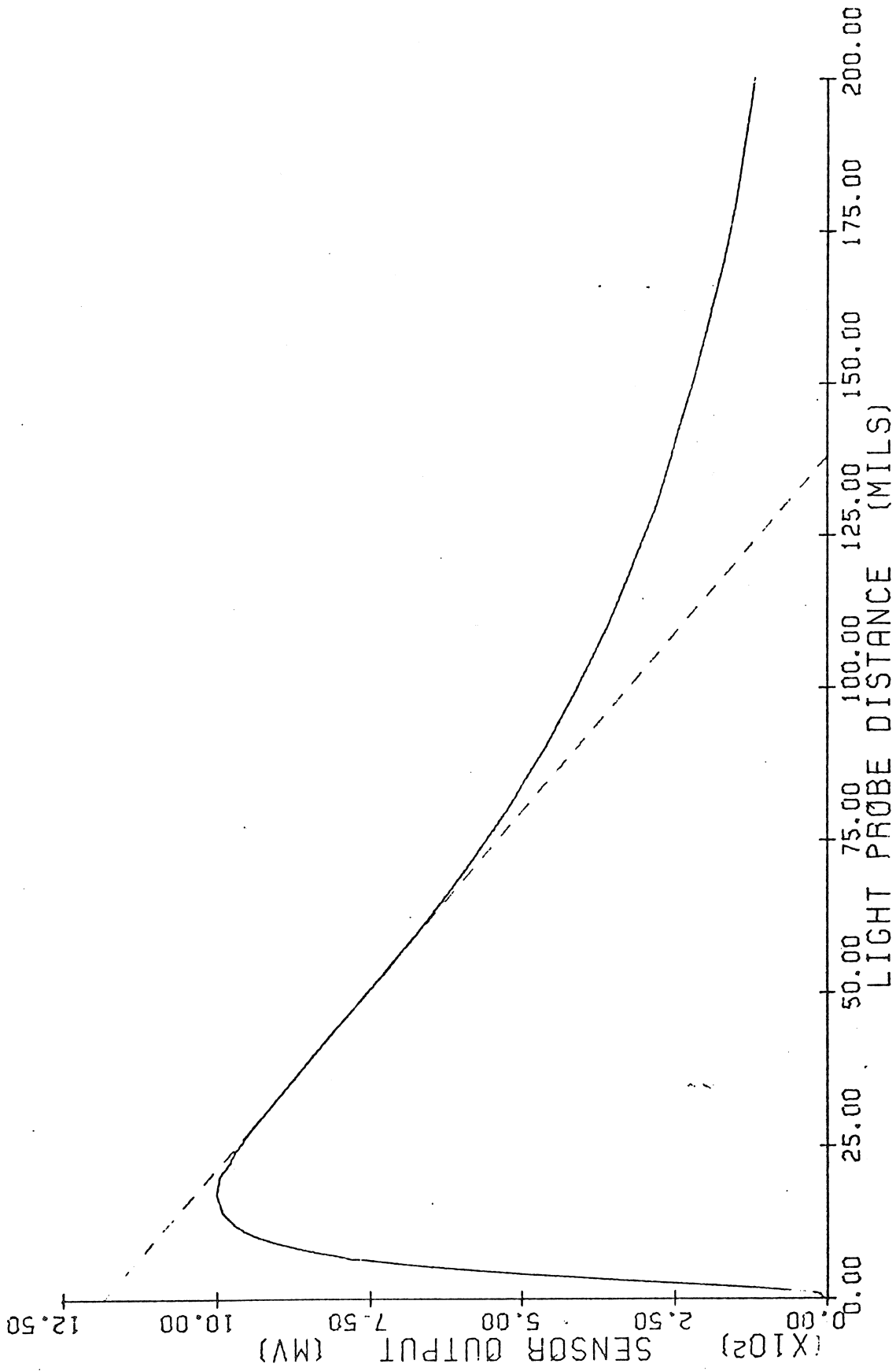


Fig. 7. Photonic sensor characteristic curve.

limp diaphragm. Comparing the theoretical high-frequency asymptotic value calculated from the enclosure volume and our experimental value from the Fotonic sensor, we found good agreement provided the diaphragm did not become too loose and distort as it deflected.

Using a paraboloid approximation for the diaphragm deflection volume (1/2 the volume of a cylinder of the same base area and height), we find the following conversion formula from Fotonic sensor output (v_f in mV) to enclosure pressure difference (Δp)

$$\Delta p = \frac{\gamma P A_d S_b}{2 V_p} v_f \quad (3-1)$$

The Fotonic sensor sensitivity is represented by S_b (m/V). A_d is the pickup diaphragm area; V_p is the pickup chamber volume; and the factor of 2 arises from the paraboloid approximation. Equation (3-1) was used to convert all raw data to the pressure difference data plotted in the result section.

3-3 Pressure Sensor Electronics

Additional electronics were added to the optical sensor output to condition the signal into a more readable form. The most important portions of this equipment were the low-pass filtering sections. The optical pickup would pass frequencies past 40 kilohertz and thus provide great amounts of noise on our infrasonic signals. The electronic low-pass filtering of the signal was much simpler than adding a chamber to the pressure sensor for mechanical low-pass filtering. Sharper cut-off (more poles), to eliminate undesired frequencies, can be provided more easily by electronic filters than by bulky mechanical filters. This method appears to be best unless the noise superimposed on the source signal exceeds the linear range of the optical sensor or the

limp range of the diaphragm, either of which calls for a mechanical solution (e.g. by varying the pickup volume). In addition to the low-pass filtering, high-pass filtering and amplification of the signal were provided for. (A circuit diagram and description of the electronics package is provided in Appendix C).

Much higher orders of signal processing can be envisioned and in particular, some type of synchronous detector system is recommended to obtain signals from noise in the low-frequency end of our testing range. By utilizing a source electronic phase signal, synchronous detection could be used and is currently under development. If our signal-to-noise ratio becomes too poor for this technique, the source volume would need to be increased.

IV. TEST RESULTS

4-1 Test Areas

The infrasonic impedance tests were run in enclosures of different volumes and varying degrees of leakiness and under different weather conditions. Our testing sites are listed and named here for the reader's convenience:

- | | |
|--------------------------|-------------------------------------|
| (1) 700 ft ³ | Darkroom, Room 302, Link Hall |
| (2) 1800 ft ³ | 306C Link Hall |
| (3) 5200 ft ³ | Skytop Apartment, 229 Chinook Drive |
| (4) 5000 ft ³ | 117 Saybrook Lane Part I |
| (5) 9000 ft ³ | 117 Saybrook Lane Part I and II |

The first two enclosures are located in Syracuse University's engineering building, Link Hall. The third enclosure is one of the many identical electrically-heated apartments in the University's Skytop complex. These apartments are relatively new (1973) and are of a preformed, concrete prefab design. The last two enclosures are part of what might be considered an average house, tested with the basement closed off. Part I and II of the Saybrook Lane dwelling represents the whole house (except basement) while for Part I alone, the three bedrooms were sealed off from the remaining living area and not included in the test.

Most of the initial development was done in the darkroom of Link Hall. In addition to the dynamic tests, static tests, using the blower method, were run on most of the enclosures as a check on dynamic test accuracy.

4-2 Infrasonic Impedance Tests

Figure 8 shows the frequency response of the darkroom. The two

DARKROOM

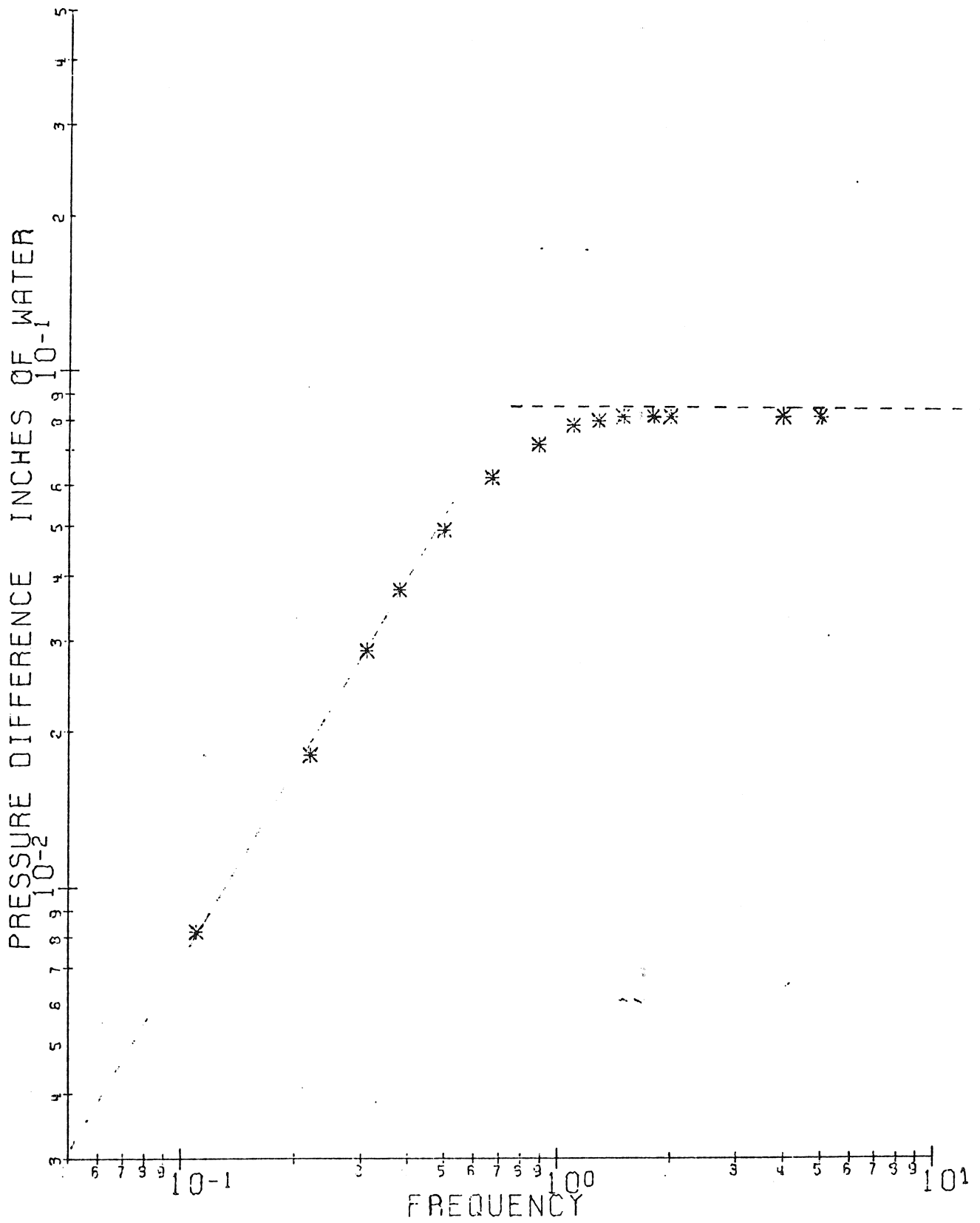


Fig. 8. Measured frequency response of Darkroom.

asymptotes intersect at break frequency $f_2 = \omega_2/2\pi = 0.7$ Hertz. The low-frequency asymptote has slope $1/n = 1.3$ thus $n = 0.77$. Substitution of ω_2 and n into Eq. (2-26) allows us to calculate our air leakage parameter K .

The darkroom test shows experimentally that the shape of the frequency response is basically that predicted by our theory.

The frequency response of Room 306C is shown in Fig. 9. The low-frequency asymptote has slope $1/n = 1.57$ or $n = 0.64$ and the break frequency is at 0.65 Hertz. During this particular test, the door was taped to allow very little leakage of air in or out of the room. If the door were untaped we would expect a shift in the response to indicate the additional leakage. Since the room volume and source displacement do not change, the high-frequency asymptote should be the same in each case; but the low-frequency asymptote should shift upwards in frequency in proportion to the increase in leakage. Fig. 10 is the graph shown in Fig. 9 and in addition we show the shifted response of Room 306C with the door untaped. A change in slope would generally be expected along with the shift because no control is made on the type of flow in the added leaks.

The added leakage in the enclosure seems to have caused another and unexpected change in our frequency response. We find the response exceeds the value of the high-frequency asymptote then finally settles to the asymptotic value at a much higher frequency. The best explanation for this overshoot in the frequency response curve seems to be that a resonant effect is taking place as almost any other effect would cause a decrease in the response. Our explanation of this overshoot is an inductive or inertial effect caused by the mass of air as it flows in and out of

ROOM 306C

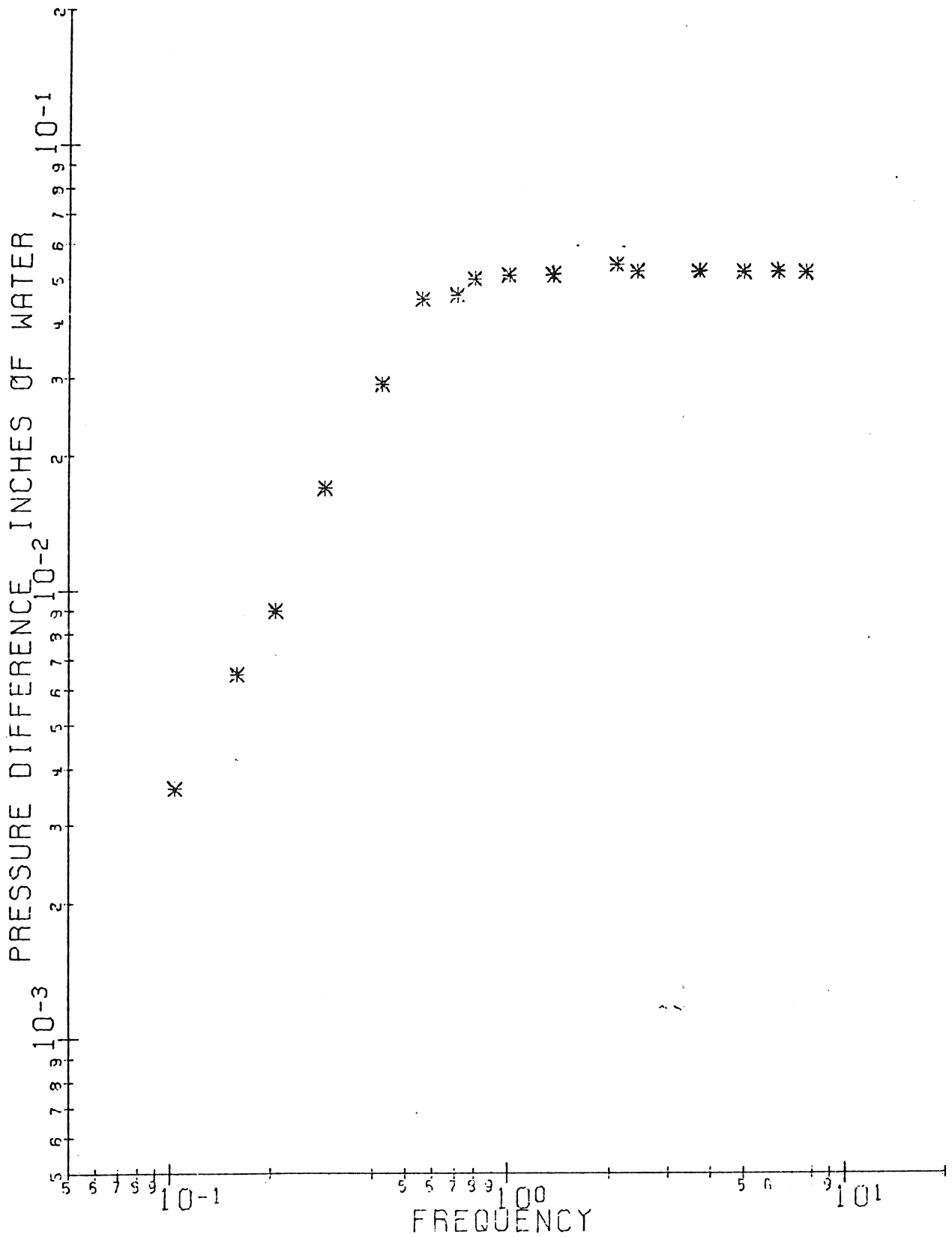


Fig. 9. Frequency response of 306C Link Hall.

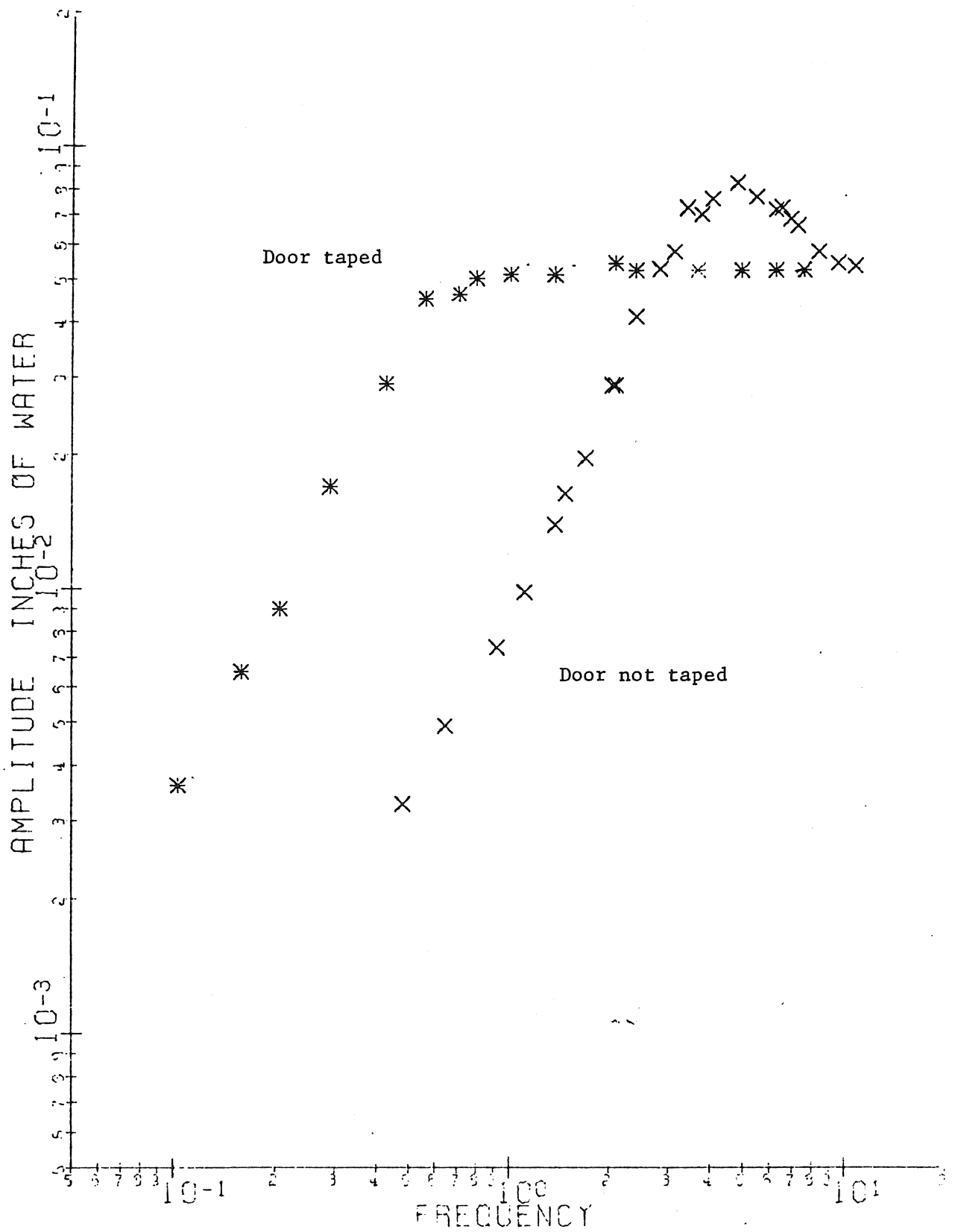


Fig. 10. Room 306C under different conditions.

the enclosure. Our circuit model, shown in Fig. 3, could be modified by including an inductance in series with the nonlinear resistance. Figure 11 shows the frequency response of such a circuit for different values of inductance. The addition of the inductance generally complicates our model's response but it does not shift the break frequency, and our analysis can proceed ignoring the inductance as long as a good approximation for the low frequency asymptote can be obtained.

When testing the larger volumes at Skytop and 117 Saybrook we found our signal-to-noise ratio was smaller, as expected. This caused greater scatter in the data and less sensitivity to changes in the amount of leakage. Figure 12 shows two test curves from Skytop. The first curve (the lower one) was taken with the kitchen and bathroom vents closed off. When the vents were opened our performance curve shows a slight shift in break frequency. Had the open vents been larger, or had they contributed a greater part of the leakage, a more definite shift would have occurred.

The curves in Fig. 13 show two tests on different volumes at 117 Saybrook Lane. As with Skytop, the leakage was so large that the high-frequency asymptote was never reached. As in all cases, however, this asymptote can be calculated from the source and enclosure volumes. If the angular speed of the source were large enough, the experimental and theoretical values for the high-frequency asymptotes could have been used as a system check. In all cases we had close agreement except in small volumes where we believe wall movement may have decreased our pressure difference in the enclosure. The mechanics and effects of wall movement could be modelled by a series RLC circuit in parallel with the capacitor in Fig. 4.

INDUCTANCE

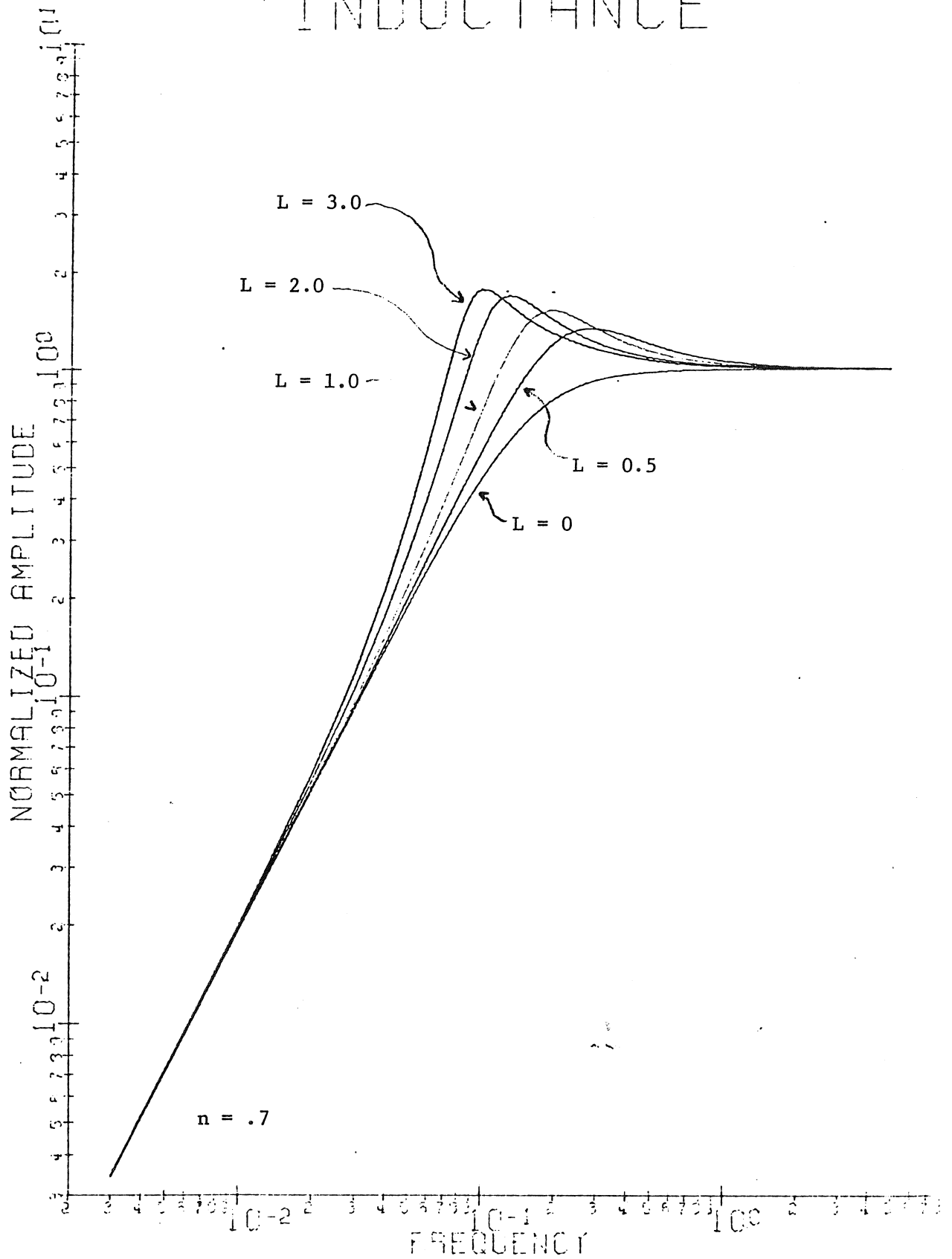


Fig. 11. Frequency response with different inductances.

SKYTOP

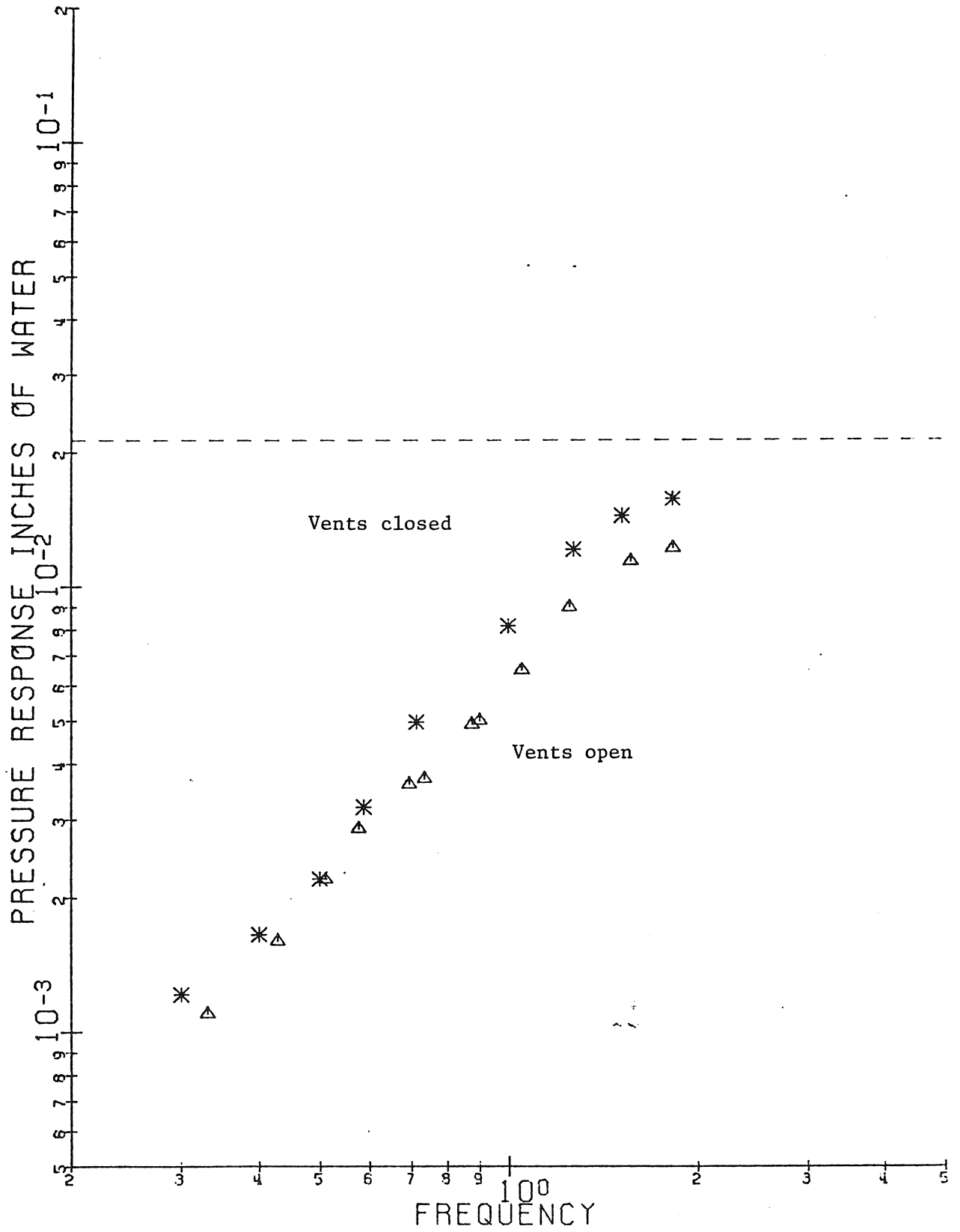


Fig. 12. Frequency response of a Skytop apartment.

117 SAYBROOK

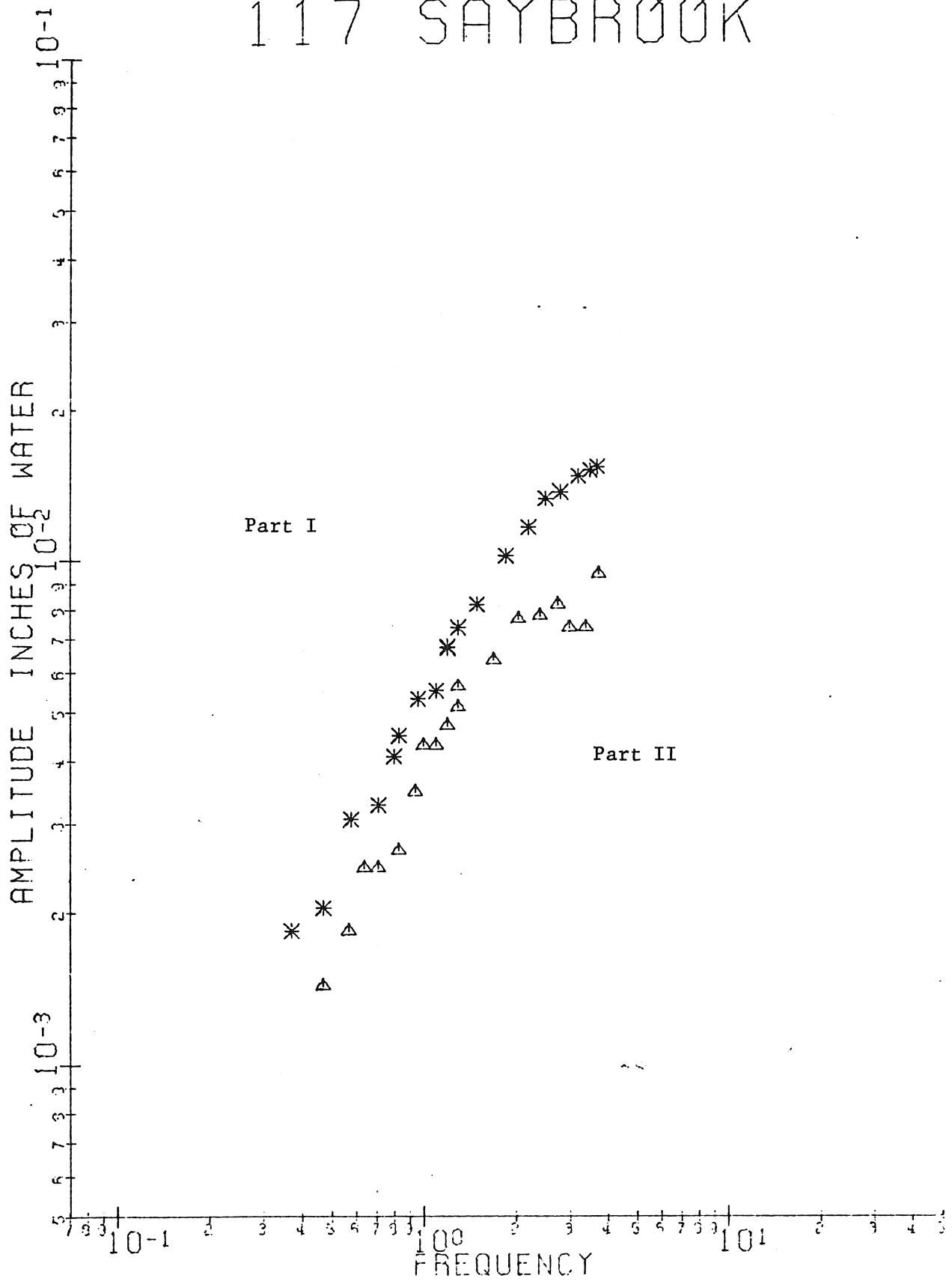


Fig. 13. Frequency response of 117 Saybrook Lane.

4-3 Blower Test Results

Figure 14 shows the test results of the blower method on Room 306C Link Hall. This graph is characteristic of the data obtained for all the enclosures tested using the blower method. The data shows more scatter than expected and work is underway to increase the accuracy of the blower method results.

4-4 Discussion of Results

Table II shows some of the important parameters and test results of the enclosures. To provide a standard for comparison, the leakage is calculated at 24.9 N/m^2 (0.1 in water) and shown in the last two columns for both the blower and infrasonic impedance methods. The values of C are calculated from our volume estimates and may be in error due to building irregularities and contents. Agreement with high-frequency asymptotes show the capacitances to be fairly close, however. The break frequency and n values come from curve approximations of the pressure response graphs. The n values compare very well, the largest error being only about 13%. K is calculated using Eq. (2-26) for the infrasonic impedance method. Once K has been established, the flow can be determined for any pressure using Eq. (2-10) and a graph of flow versus pressure (as in Fig. 14) can be obtained.

In the comparison of our flow at 24.9 N/m^2 (0.1 in water) on table II, there is considerable error. The error exists mainly in the larger enclosures where the data is more scattered and less reliable. The blower and infrasonic impedance tests were run under different conditions for 306C. When the infrasonic test was run with the same condition as the blower test, a break frequency of 0.38 Hertz was obtained and a flow of $0.014 \text{ m}^3/\text{sec}$ resulted. This is very close to the blower

306C

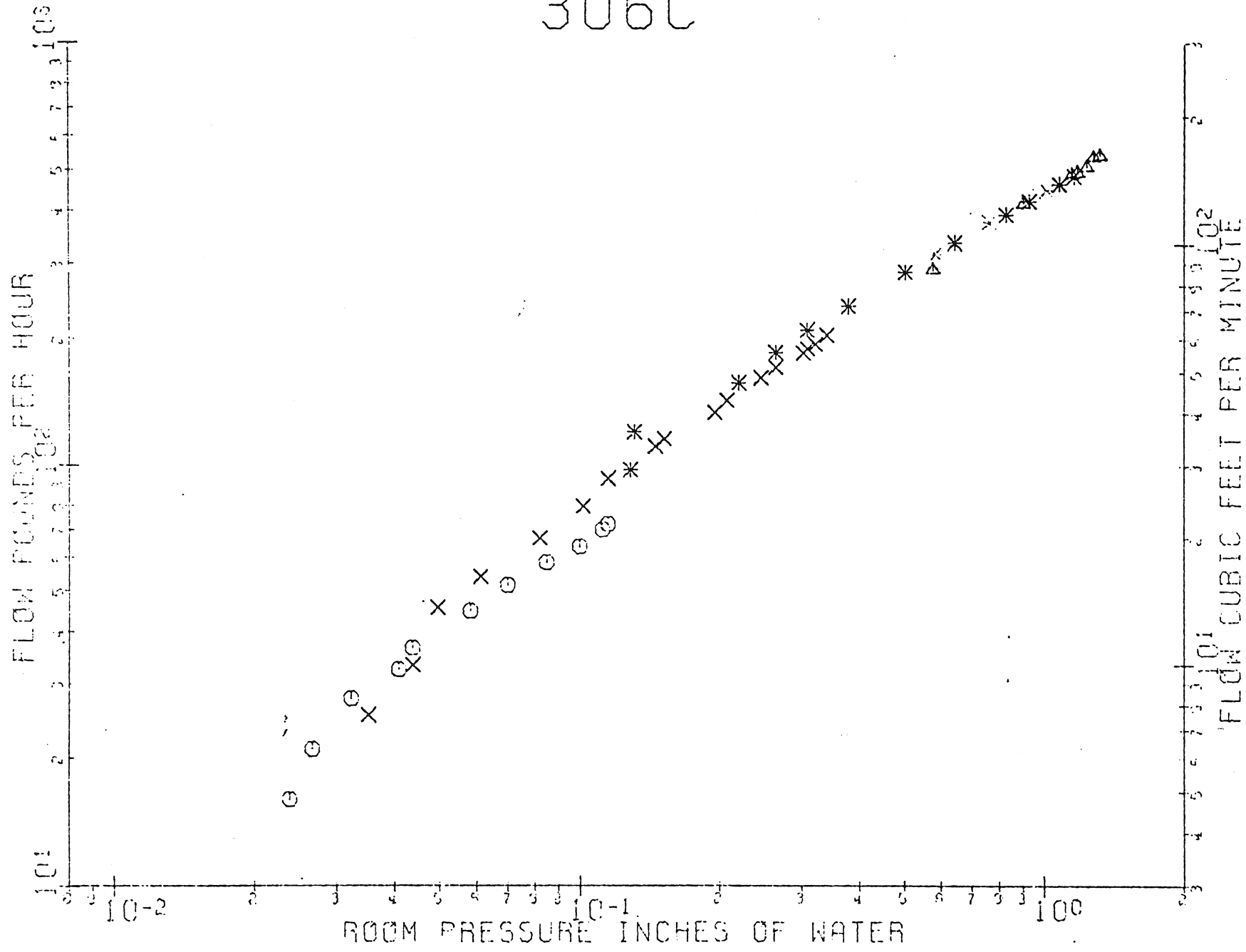


Fig. 14. Blower test curve for 306C Link Hall.

TABLE II

	Volume m^3	Acoustic Capacitance m^5/N	Break Frequency Hz	n Infrasonic Tests	n Blower Tests	K Infrasonic Tests	Blower Test Q* m^3/sec	Infrasonic Test Q* m^3/sec
Darkroom	20	1.4×10^{-4}	0.7	0.77	None	1.2×10^{-3}	None	0.015
306C Link Hall	50	3.6×10^{-4}	0.65	0.64	0.65	3.1×10^{-3}	0.013	0.024
Skytop 229 Chinock Dr.	150	1.1×10^{-3}	2.8	0.70	0.66	2.5×10^{-2}	0.22	0.23
117 Saybrook Lane Part I	142	1.0×10^{-3}	3.8	0.84	0.74	2.6×10^{-2}	0.16	0.46
117 Saybrook Lane Part I and II	255	1.8×10^{-3}	3.0	0.89	0.87	3.6×10^{-2}	0.30	0.63

* Flow at a room pressure of 0.1 inch of water.

test result. At Skytop good agreement resulted even with scattered data. At 117 Saybrook Lane, infrasonic impedance data was scattered and blower test problems make both data sets unreliable. No blower test has yet been run on the darkroom to compare values. There may be significant error in blower test results for very low flow rates as the flow at these low rates is less than expected from Eq. (2-10). The low reading might be caused by leakage into our blower system.

V. PRESENT WORK AND RECOMMENDATIONS

5-1 Experimental Work and Recommendations

Under development now is a system using a type of synchronous detector to obtain a strong, accurate signal even in a noisy environment. A photo detection setup will feed source phase information to our electronics for higher level processing of the pressure sensor signals.

The blower system needs work to determine the reasons for the scatter in data. Results of blower tests are discontinuous when nozzles (for flow measurement) are changed. More accurate blower tests would show if the error truly is in the infrasonic tests.

A redesign of the source with a two-speed or three-speed gearbox and direct drive would make frequency range changes easier and perhaps a broader frequency spectrum possible.

Increasing the source volume would provide better signal to noise ratios in larger buildings and perhaps improve the results there.

5-2 Theoretical Work and Recommendations

Wall movement has been evident in several locations. The exact effect the movement has had on our results is not entirely understood. Work will need to be done to determine whether our modeling of the wall movement as a series RLC leg in our circuit model is correct and if it affects our results.

The overshoot seen in Fig. 10, is believed to be caused by an inductive (inertia) effect of the air in the leaks. The model of this will need to be proved and perhaps development of computer programs might help process data as our circuit model becomes more complex.

VI. CONCLUSION

The infrasonic impedance of a building, as far as is known, has never been used before our work to determine the air leakage property of a building. In fact, we believe, the tests on our enclosures represent the first time infrasonic building impedance has been measured for any purpose. For small enclosures the results follow the theory very closely and agree with the tests made by the conventional blower method. Up to now, when working in larger volume enclosures, the smaller signals received yield more scattered data and give results which are large by a factor of two or more compared with the blower tests. The values obtained for n , the reciprocal of the slope of the log-log plot of the low frequency asymptote, showed excellent agreement between the blower and infrasonic methods. The largest error was only 13% even for scattered data and large enclosures.

The infrasonic impedance testing method has several advantages over the conventional air leakage testing methods. An infrasonic test with present apparatus can be run in much less time, commonly 20 minutes compared to 90 minutes or more for blower tests. Less time is needed for equipment setup as no external venting is needed. Less operator skill is needed once equipment is set up, leaving less room for error.

The infrasonic impedance tests have demonstrated that air leakage can be measured in small volume enclosures. The system shows promise of good correlation between the blower and infrasonic test results when used in larger volumes.

APPENDIX A

Solution of Equation (2-13)

Equation (2-13) is repeated here for the convenience of the reader.

$$C \frac{d}{dt} \Delta p(t) + K \frac{\Delta p(t)}{|\Delta p(t)|} |\Delta p(t)|^n = q_s(t) \quad (A-1)$$

The above nonlinear equation is easiest solved numerically on a computer. An iterative scheme using the Taylor series expansion was developed to calculate distinct values of the solution in the region of the break frequency. Values were also calculated in the asymptotic region as a check on our program. The program was also used to calculate values in the linear case and, as expected, the values obtained agreed with those predicted by Eq. (2-14), the linear equation.

The nonlinear steady state normalized numerical solution was then approximated by the following equation:

$$\Delta p(t) = \frac{\omega^{1/n}}{\sqrt{1 + \omega^{2/n}}} \quad (A-2)$$

where $\Delta p(t)$ is the amplitude of the response for a given angular frequency ω and exponent n . Equation (A-2) has the same asymptotes as the nonlinear case and reduces to our linear equation when $n = 1$.

Figure A-1 shows a graph of Eq. (A-2) and also a series of points calculated by our computer solution of Eq. (A-1). In the worst case, agreement is better than 5 per cent and consequently we shall use the approximation curve Eq. (A-2) as our solution. Figure 6 shows graphs of our approximate solution for different values of n .

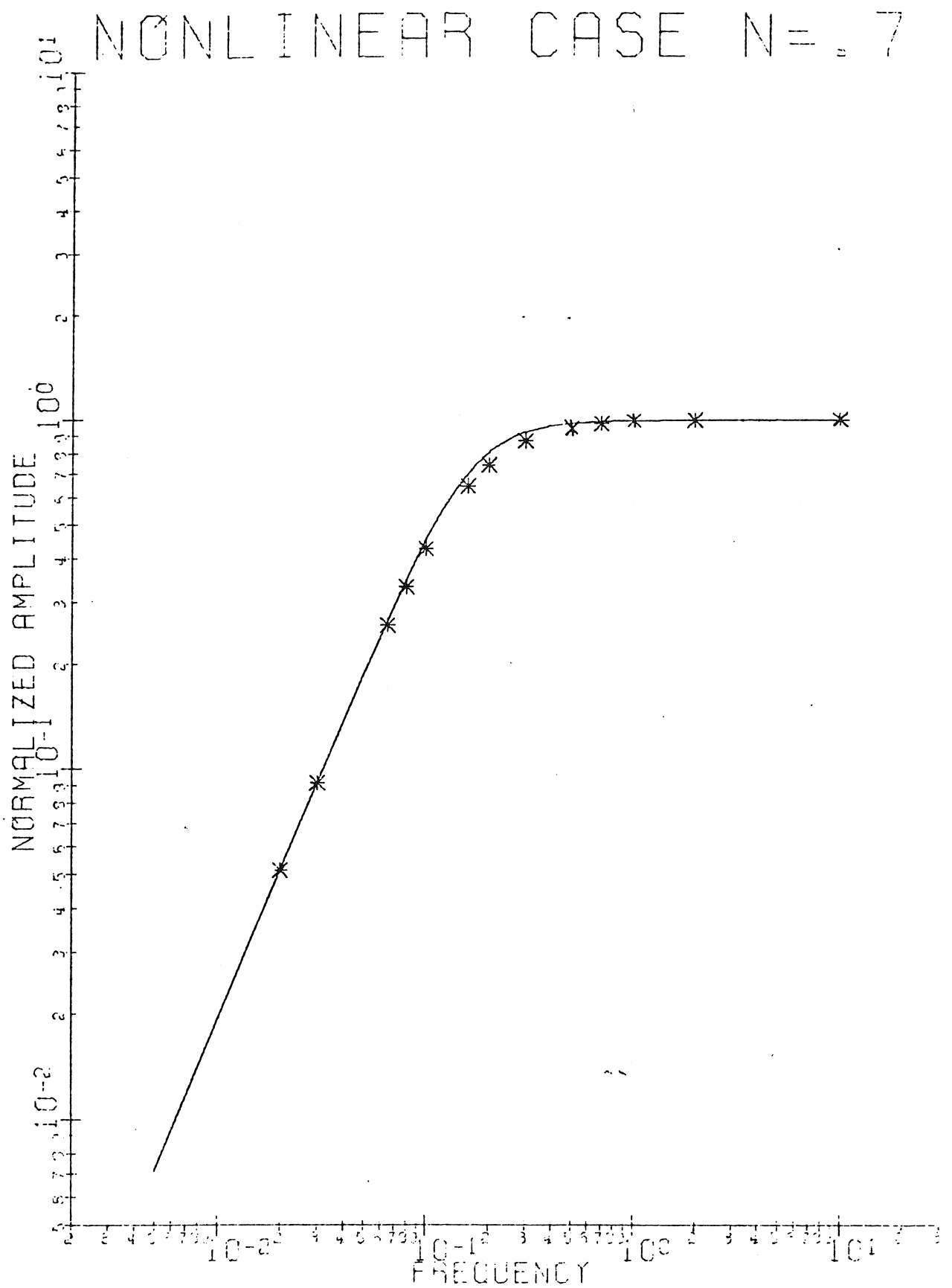
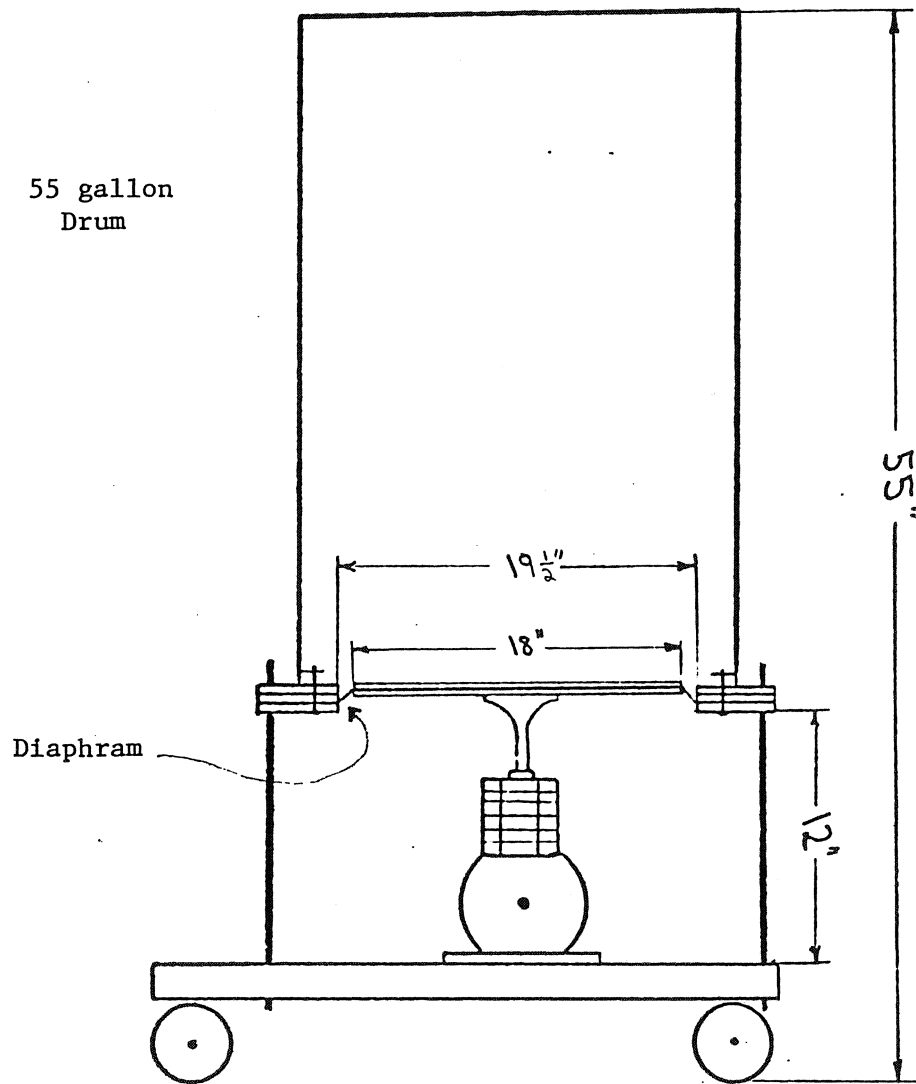


Fig. A-1 Approximate nonlinear solution (solid line) shown with points from numerical solution.

APPENDIX B

Volumetric Flow Source and Equipment

Figure B-1 shows a scale drawing of part of the pressure source diaphragm pump. For simplicity the gearbox pulleys, motor and controls are not shown here. The specifications of most of the equipment used are given in Table B-1 and the motor control circuit is shown in Fig. B-2. The use of a d-c motor with armature voltage control allows wide speed variation in order to give a broad frequency response. Ideally, a voltage-source drive would keep the motor speed constant regardless of the cyclic torque fluctuation imposed on the motor by the pump. The reactor in the armature control acts to smooth the full-wave-rectified current from the diode bridge. Further speed changes can be made by pulley and belt changes on the motor and gearbox allowing an even wider frequency response. Typically two pulley changes gave a range of 0.1 to 10 Hertz when used along with the d-c motor control. Slower speeds of the motor would cause the source signal to become slightly non-sinusoidal.



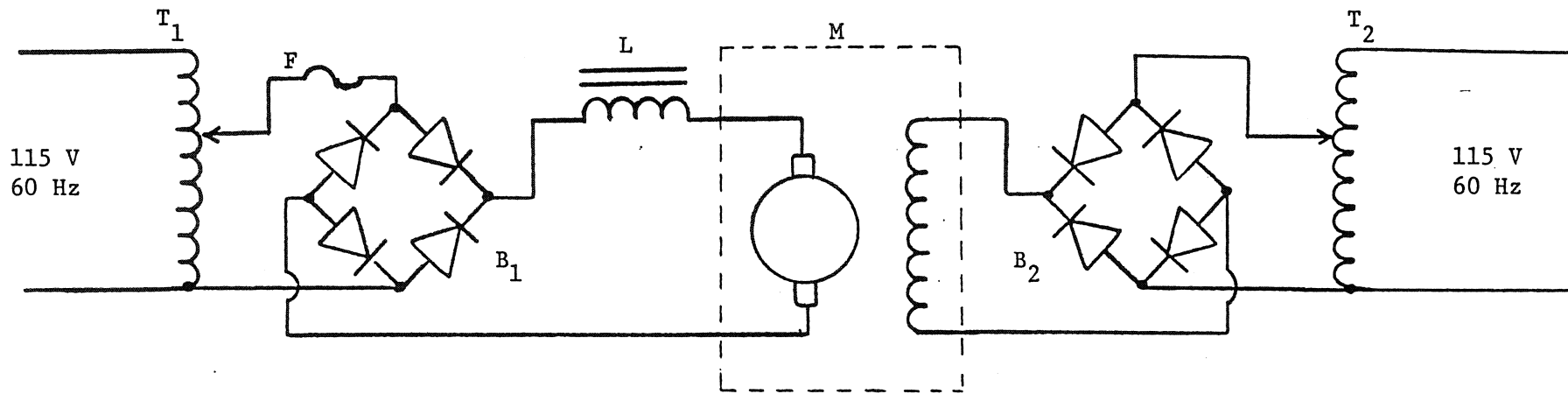
Scale 1:10

Fig. B-1 Scale drawing of pump source (No motor, gearbox, belts or controls are shown).

TABLE B-1

Equipment

1. Fotonic Sensor MTI Model KD-38
Mechanical Technology Incorporated
968 Albany-Shaker Rd., Latham, NY 12110
2. Two channel high speed recorder
Gulton techni-rite electronics Model TR-722
3. DC Generator (used as shunt motor)
Westinghouse type FK Frame D185
style 1172247-B 40 Volts 2000 RPM
4. Speed reduction gearbox
Ohio Gear Co. #8HU- 5 1/6 C
reduction ratio 5 1/6 to 1
5. Crank mechanism
3 H.P. lawnmower engine
stroke 1.5 inches T.D.C. to B.D.C.
6. Pump diaphragm
1/32 inch gum rubber.
7. Pickup diaphragm
Saran wrap plastic film thickness = 1×10^{-5} m (.4 mils)
8. Belt ratios- variable by pulley changes in series with 5 1/6 to
1 gear reduction, 1.3 to 1, 2.8 to 1, 4.1 to 1, 5.4 to 1



T₁ 10 Amp Variac
 T₂ 5 Amp Variac
 F 10 Amp Fuse ;

B₁ 10 Amp diode bridge
 B₂ 4 Amp diode bridge
 L 25 mH, 0.425 ohm d-c Res.
 M D-C Shunt Motor

Fig. B-2 Motor Control Circuit

APPENDIX C

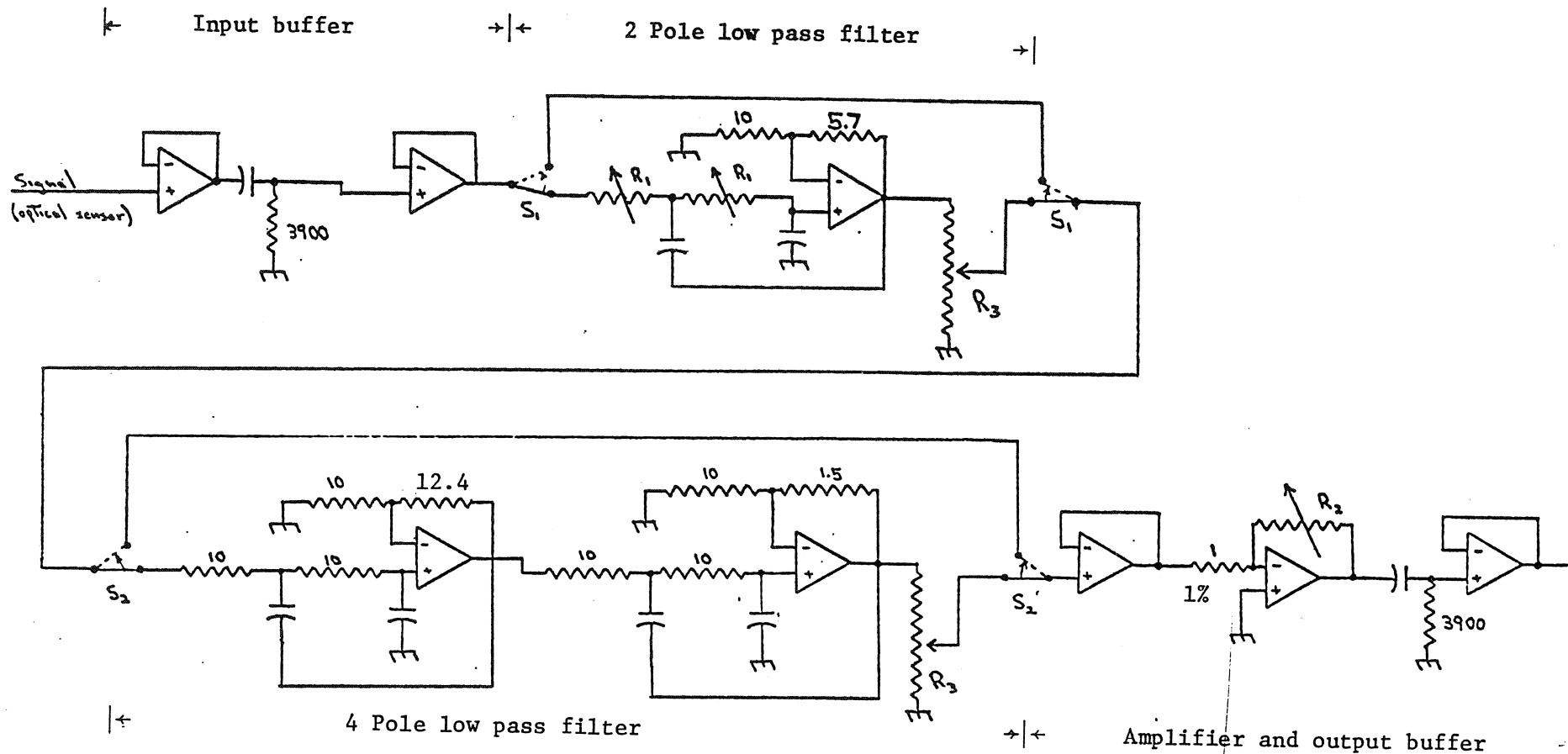
Signal Processing Circuit

Figure C-1 shows the electronics package used to process the signal from the optical pickup. Connection is made from the Fotonic sensor pickup by a shielded lead to the input buffer. Included in the buffer is a high-pass filter with a break frequency (pole) at 0.018 Hertz. The high-pass filter attenuates noise at frequencies below our range of interest and also provides d-c blocking. The d-c blocking is needed because, as shown in Fig. 7, the linear range of the back side of the Fotonic sensor has a d-c offset of about 0.8 volts.

The second section of the electronics is an adjustable-break-frequency two-pole low-pass filter. Switch S_1 allows this stage to be bypassed completely for calibration or if filtering is not desired. Rotary switch R_1 allows different resistances to be used in order to shift the break frequency for maximum filter benefit.

The next section is a four-pole, low-pass filter with break frequency at 7.2 Hertz and switch S_2 to bypass this filter if higher frequency excitations are used. Both low-pass filter sections are Butterworth designs and provide no overshoot and a maximally-flat frequency response. Figure C-2 shows the frequency response of our entire electronics package with the adjustable two-pole filter pole at 7.2 Hertz and a gain of one.

Following the filter stages are the amplifier and output buffer. An operational amplifier (op amp) voltage follower prevents filter loading and feeds an inverting amplifier. The high-pass filter on the amplifier output provides blocking of the accumulated d-c offsets of the type 741 op amps while the follower prevents loading and acts as a chart recorder



S_1 - 2 pole filter switch DPDT

S_2 - 4 pole filter switch DPDT

R_1 - 3 pole rotary switch
 $R = 2.2, 10$

R_2 - 2 pole rotary switch
 $R = 1, 2, 4, 10, 15, 20, 30, 50 (1\%)$

R_3 - 10K Trimpots

All resistances in kohms

All capacitors are $2.2 \mu\text{F}$

All operational amplifiers are MCL741CP

Fig. C-1 Signal Processing Circuit.

FREQUENCY RESPONSE

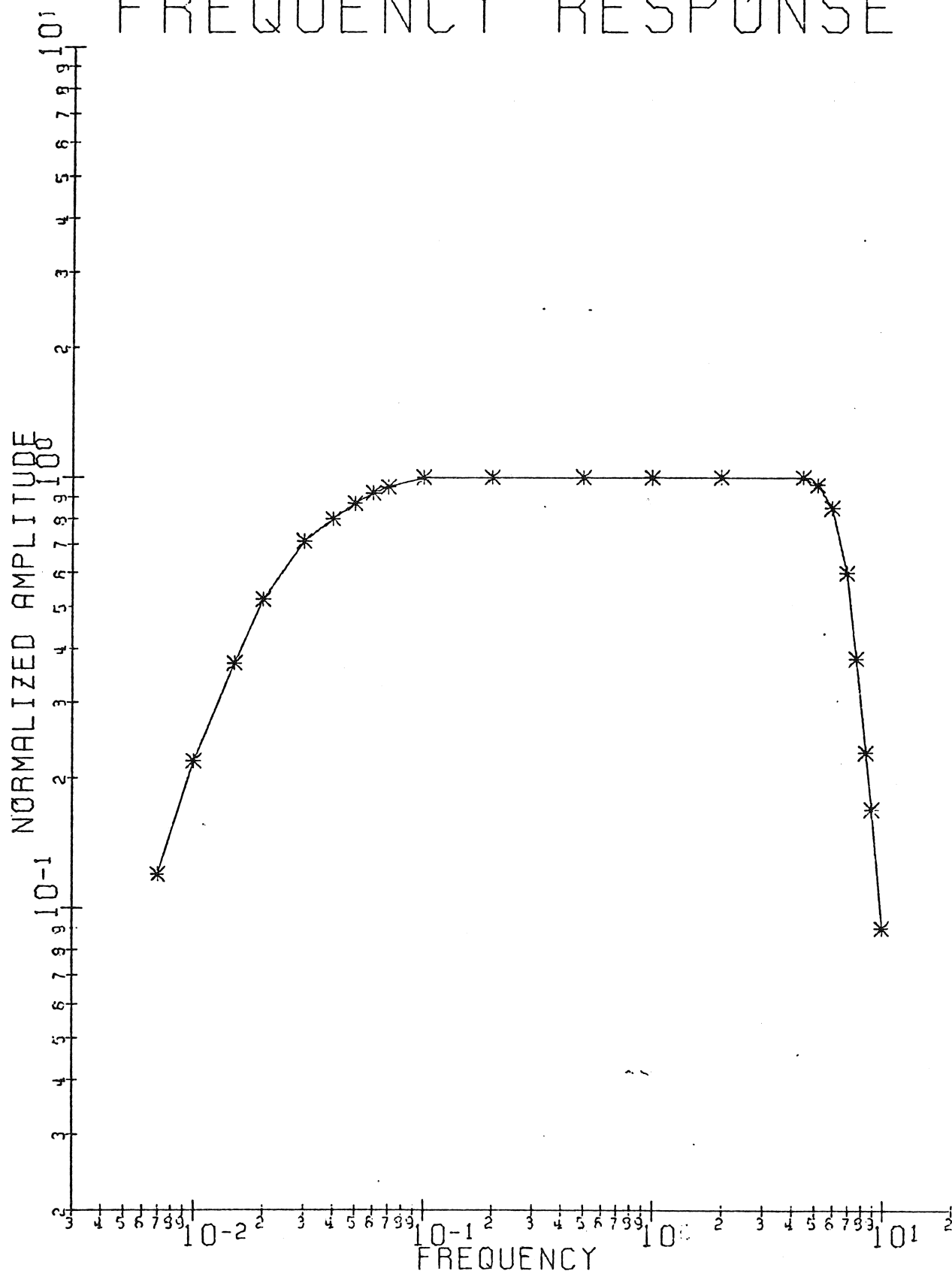
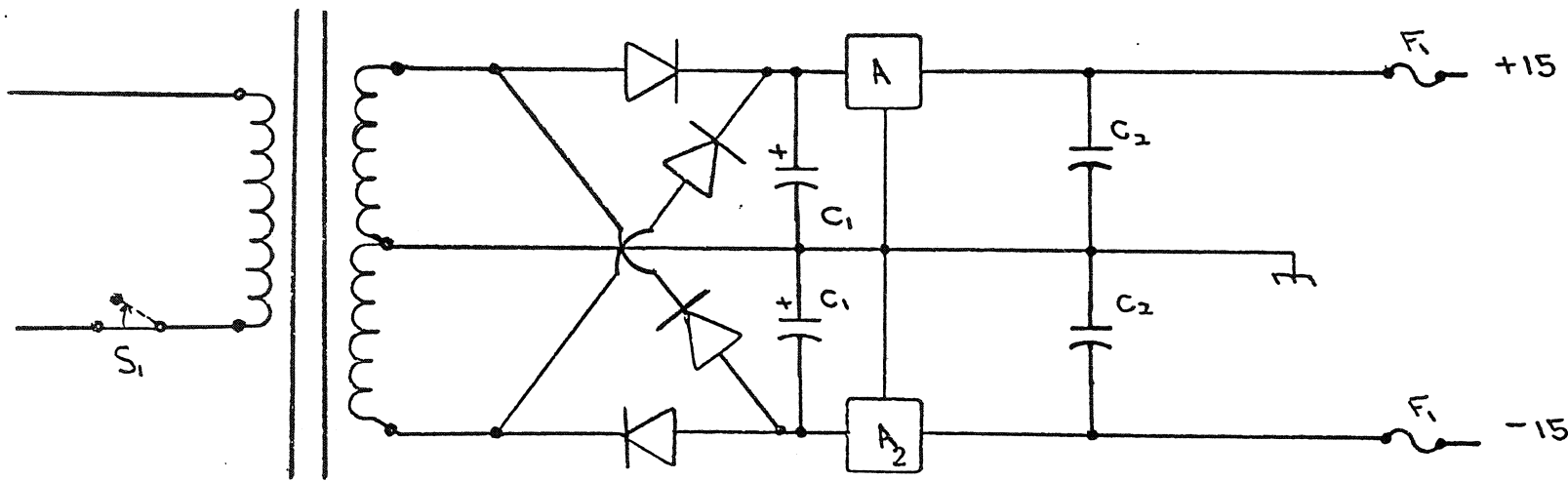


Fig. C-2. Frequency response of total electronic package.

driver. The amplifier section provides step gain by means of rotary switch R_2 which switches in different valued feedback resistors.

The entire circuit package was designed with flexibility and expansion in mind. The buffers are included so as to assure no loading of stages which might provide incorrect results. The package works quite well although the high-pass filter sections require about 10 seconds to stabilize to steady-state values.

Figure C-3 shows a schematic of the electronic power supply. Design was a simple full-wave-rectified, integrated-circuit-regulated supply. The circuit is fuse-protected and designed for 1 ampere at plus and minus 15 volts d-c.



All diodes are 1N4004

C_1 - 5600 μ F 25VDC

C_2 - 2.2 μ F

S_1 - SPST

F_1 - 1 amp fuse

A_1 - LM 340-15

A_2 - LM 320-15

T_1 - Stancor 36 v CT 1 amp Transformer

Fig. C-3. Power supply.

REFERENCES

- [1] Patterns of Energy Consumption in the U.S., Office of Science and Technology Executive office of the President, Washington, D.C., 1975.
- [2] ASHRAE Handbook of Fundamentals, American Society of Heating, Refrigerating and Air-Conditioning Engineers, 345 East 47th Street, New York, NY 10017, 1972 pp. 381-383.
- [3] John M. Fox, Energy Consumption for Residential Space Heating--A Case Study, Princeton University, School of Engineering and Applied Science Center for Environmental Studies, Princeton, NJ 08540, Report No. 4, Sept. 1, 1973, p. 29.
- [4] Robert H. Socolow, Efficient Use of Energy, Physics Today, August 1975, pp. 23-39.
- [5] B. B. Bauer, Equivalent Current Analysis of Mechano - Acoustic Structures, Journal of the Audio Engineering Society, Oct. 1976, Vol. 24, #8, pp. 645-646.
- [6] *ibid*, pp. 646-647.
- [7] C. Y. Shaw, D. M. Sander, and G. T. Tamura, Air Leakage Measurements of the Exterior Walls of Tall Buildings, ASHRAE Transactions, Vol. 79, 1973, p. 337.

- [8] G. T. Tamura and A. G. Wilson, Building Pressures Caused by Chimney Action and Mechanical Ventilation, ASHRAE Transactions, Vol. 73, part II, 1967, pp. II.2.1-II.2.12.
- [9] R. C. Murtz and M. J. Curry, Microbarograph for Meteorological Studies: Design, Theory, and Analysis, Journal of Physics E: Scientific Instruments, 1971, Vol. 4, pp. 307-310.

BIOGRAPHICAL DATA

Name: R. W. Graham

Date and Place of Birth: June 13, 1953
Philadelphia, Pa.

Education:

High School: Henderson High
West Chester Pa., 1971

College: Syracuse University
Syracuse, N.Y., 1975

Graduate Work: Syracuse University
Syracuse, N.Y.
Graduate Assistant, 1975-1977